Piloted Flight Simulation of Helicopter Recovery to the Queen Elizabeth Class Aircraft Carrier

Neale A. Watson,[1] Ieuan Owen,[2] and Mark D. White[3]
School of Engineering, Liverpool, L69 3GH, United Kingdom

This paper describes how flight simulation has been used to investigate helicopter recovery operations to the deck of HMS Queen Elizabeth, the UK's new aircraft carrier. A helicopter flight simulation environment has been developed in which the unsteady air flow over the ship has been created using full-scale Computational Fluid Dynamics. A six degree-of-freedom motion flight simulator has been used to conduct real-time piloted deck landings where a helicopter flight dynamics model representative of a Sikorsky SH-60B Seahawk helicopter was recovered to the designated rotorcraft landing spots towards the stern of the ship. A test pilot was instructed to land the helicopter and to give workload ratings for the difficulty of the task when flying in relative winds from ahead, and 45° and 90° from starboard. The workload ratings, along with the corresponding pilot control activity and helicopter positional accuracy, are discussed in relation to the air flow to which the helicopter was subjected. The paper demonstrates how flight simulation could be used to support flight trials and helicopter clearance activities, but also notes that real-world trials data is needed to compare with the simulations before the techniques can be beneficially deployed.

I. Introduction

HMS Queen Elizabeth, commissioned in December 2017 and shown in Fig. 1, is the first of United Kingdom's two new Queen Elizabeth Class (QEC) aircraft carriers and, at the time of writing, has recently successfully undertaken sea-trials and First-of-Class Flight Trials (FOCFTs) for both rotary-/fixed-wing aircraft. The QEC, with a length of 280m, a beam of 73m and a displacement of 65,000 tonnes, is the largest warship ever built for the Royal Navy. While

[1] Ph.D. Candidate, School of Engineering
[2] Emeritus Professor of Mechanical Engineering, School of Engineering
[3] Professor of Aerospace Engineering, School of Engineering

the QEC has primarily been designed to operate the Lockheed Martin F-35B Lightning II Short Take-Off and Vertical Landing (STOVL) stealth fighter jet [1], it will also operate a range of rotary-wing assets such as Merlin, Wildcat, Chinook and Apache helicopters.

Characteristic features of the QEC, as can be seen in Fig. 1, are the two islands on the starboard side of the flight deck and the take-off ramp, or ski-jump, at the front of the ship. The forward island is responsible for ship control and navigation, whereas the aft island houses an area known as Flying Control, or FLYCO, and is responsible for directing flight operations. The ski-jump at the bow is to facilitate a short take-off by imparting an upward vertical velocity and ballistic profile to the STOVL fixed-wing aircraft, providing additional time to accelerate to take-off whilst ensuring it is on a safe trajectory [2].

Fig. 1 Royal Navy Wildcat Helicopter above HMS Queen Elizabeth © Crown 2017.

Preparation for the fixed-wing flight trials was greatly assisted by use of modelling and simulation where a flight simulation facility was developed at BAE Systems, Warton, specifically to support the F-35B/QEC clearance and qualification process [3]. The use of piloted flight simulation in preparing for the trials represented a significant milestone in the application of modelling and simulation to the launch and recovery of ship-borne aircraft. The purpose of the present paper is to describe a parallel study in which rotorcraft flight simulation trials were conducted independently at The University of Liverpool (UoL) as a research activity. The study is part of ongoing research into

modelling and simulation of the ship-helicopter dynamic interface [4], and did not contribute directly to the helicopter/QEC FOCFTs.

The environment around the ship's landing deck is known as the dynamic interface, which reflects the time-varying and volatile nature of the conditions faced by the pilot and aircraft during operations close to the ship's deck and superstructure [5]. The disturbed air flow over a ship's superstructure is commonly known as the 'airwake' and is caused by a combination of the ship's forward speed and the prevailing wind [6]. A significant body of research has been conducted in an effort to understand ship airwakes, particularly for single-spot ships; a comprehensive review is provided by Shukla et. al [7]. As computing power has increased, focus on ship airwake modelling has shifted from experiments to Computational Fluid Dynamics (CFD), allowing high Reynolds number flows to be resolved numerically [8 -10]. To capture the time-dependent velocity fluctuations present in a ship's airwake, an unsteady CFD solver is required to resolve the turbulent flow field, e.g. [11, 12]. CFD modelling of the flow over multi-spot aircraft carriers presents a particular challenge due to the large mesh cell count required for such large ships with complex geometries [13]. Polsky et al, using the commercial CFD code COBALT, computed a time-accurate solution of the flow over an US Navy LHA class ship, which showed good agreement with wind tunnel velocity measurements [14]. The characteristic geometry of aircraft carriers, i.e. large flat flight decks with single or twin island superstructures and, possibly, ski-jumps, create unique flow structures that can significantly affect aircraft during take-off and landing [15-18]. During the period of development of CFD-generated ship airwakes, it has also been recognised that such airwakes could contribute to the development of realistic simulation environments that include the unsteady air flow over the ship and its interaction with the ship-borne aircraft [19-23].

Previous research at UoL has focused on helicopter operations to single-spot frigates and destroyers with the overall aim of maximising operational capability and reducing pilot workload during helicopter launch and recovery by: (i) creating a flight simulation environment for realistic helicopter launch and recovery operations [24], and (ii) developing guidance for ship designers to minimise the effect of ship superstructure aerodynamics on helicopter operations [25-26]. This paper will describe a flight simulation environment that was developed to enable simulated piloted flight trials for a helicopter being recovered to the QEC and will present the results of those trials for a selection of challenging wind conditions.

II. Flight Simulation Environment

High-fidelity piloted flight simulation for helicopter landings to a ship ideally requires a six degree-of-freedom motion flight simulator to provide motion and visual cues to the pilot in the highly dynamic flying environment over the ship's deck. It also requires effective modelling of the helicopter's flight dynamics, unsteady ship airwakes, and ship motion, along with realistic visual models, including sea surface, ship geometry, deck markings, and visual landing aids.

Fig. 2 QEC visual environment in the HELIFLIGHT-R flight simulator.

HELIFLIGHT-R, Fig. 2, is a fully reconfigurable research simulator [27], consisting of a generic rotorcraft crew station housed inside a 12ft diameter visual display dome, mounted on a motion platform. The platform is a standard hexapod configuration, comprising six electric actuators, each with a 24in stroke. The simulator cabin houses a twin-seat cockpit, with a third seat at the rear for an instructor or simulator operator. The primary cockpit instruments are presented on two wide-screen flat-panel displays. A four-axis electronic control loading system provides the capability to configure the force-feel characteristics of both the pilot and co-pilot's cyclic, collective and pedal controls to represent a wide range of aircraft types. Three Digital Light Processing (DLP) projectors, with a resolution of 2,560 × 1,600 pixels, are used to project an outside-world image onto the inside surface of the dome. The three images are geometry-corrected and edge-blended, before being projected, to present a single continuous image to the pilot in the cockpit, as can be seen on the right in Fig. 2. The projectors are equipped with wide-angle lenses and provide a horizontal field-of-view of 230° (±115°) and a vertical field-of-view of 70° (+30°/-40°). The visual scene was

simulated using Presagis Vega Prime. Audio cues are presented to the pilot using a system of loudspeakers distributed throughout the cockpit.

Integration of the aircraft flight dynamics model with the HELIFLIGHT-R simulator is achieved using Advanced Rotorcraft Technology's FLIGHTLAB software [28], which provides a library of aircraft models, including a generic rotorcraft flight dynamics model that has been configured to be representative of the Sikorsky SH-60B Seahawk. Although it is recognised that the Seahawk is not in service with the UK Royal Navy, this aircraft model was used for these simulation trials due to its strong validation [29] and extensive use during previous research at UoL. An important component of the simulation environment is the effect of the ship's airwake on the helicopter. CFD-generated airwakes can be integrated with FLIGHTLAB, enabling unsteady airwake velocities to be imposed upon the aircraft flight dynamics model at various locations on the rotor blades and airframe. During testing, the FLIGHTLAB software allows real-time data monitoring and recording which, together with in-cockpit video and audio recordings, are used for post-trial analysis.

For ship-helicopter launch and recovery operations, the maximum permissible limits for a given helicopter landing on a given ship deck over a range of wind speeds and directions must be identified. These restrictions are termed Ship Helicopter Operating Limits (SHOLs) and are required for each helicopter-ship combination [30]. The SHOLs are normally determined during the FOCFTs, a dedicated programme of at-sea testing and qualification in which the safety margins and pilot workload is assessed by test pilots during helicopter launch and recovery operations according to aircraft payload, sea-state, visibility, wind speed and direction. Limits are identified using the Deck Interface Pilot Effort Scale (DIPES) which the test pilot uses to award ratings to the difficulty of the landing task, dependent on the workload experienced from the perspective of an average fleet pilot [30]. DIPES ratings are also influenced by how close the control inputs are to their safety margin. The pilot ratings given for each landing over a range of conditions is collated and used to create a SHOL diagram which defines the helicopter-ship operational envelope for each wind speed and direction at a specified Corrected All Up Mass (CAUM). The SHOL diagram is also influenced by the deck motion, method of rotorcraft recovery and the visual environment.

The FOCFT process to determine the SHOL can be extremely costly, both financially and in the commitment of valuable assets, people and equipment over a number of weeks [31]. The opportunity to test in a suitable range of environmental conditions is heavily dependent on the prevailing wind and sea-state conditions. If these conditions do not materialise the trials may have to be extended or delayed, or the lack of testing can lead to a restricted SHOL in

which the helicopter's operational envelope is constrained; SHOL diagrams determined using similar ship/aircraft types may be used conservatively to complete a restricted SHOL but this is undesirable.

Considering the large expense and uncertainty incurred in producing SHOLs for each helicopter-ship combination, a more cost-effective method would be highly beneficial. One method of reducing these costs may be through the use of modelling and simulation of the aircraft-ship dynamic interface, as an aid to real-world SHOL testing; this is becoming a more feasible option due to the increasing fidelity of simulation through research on motion tuning, pilot modelling and coupled rotor/airwake aerodynamics [3, 32-33].

A. Airwake CFD Modelling and Validation

Previous airwake research at UoL has focused on single spot frigates and destroyers. Due to the considerably larger size of the QEC, the CFD methodology for creating the airwakes was adapted from that used and reported previously [12]; furthermore, experimental validation was required. This paper will only give a brief description of the CFD process and the experimental validation, but a more detailed description can be found in [34-35].

To provide a realistic flight simulation, particularly in terms of helicopter handling qualities and pilot workload, the irregular time-varying velocities in the airwake must be computed and applied to the aircraft flight dynamics model; this requires an effective time-accurate CFD approach. Delayed Detached Eddy Simulation (DDES) with a SST k-ω based turbulence model and third-order accuracy was employed using ANSYS Fluent as the CFD solver; this time-accurate method is suitable for unsteady flow dominated by both quasi-periodic large-scale structures and chaotic small-scale turbulent features typical of bluff body geometries [36]. DDES is a hybrid approach to turbulence modelling where Large Eddy Simulation (LES) is used away from the surfaces of the ship to directly compute the larger scale turbulent structures, while closer to the surface Unsteady Reynolds-averaged Navier-Stokes (URANS) is used [37]. The method is particularly well suited to ship airwake modelling as in regions of interest, such as over the landing deck, the turbulent features are explicitly resolved. Also, compared with a "pure" URANS approach, DDES has less dissipation of turbulent kinetic energy in the flow shed from the bluff superstructure.

The QEC's landing deck encompasses a large area and the CFD method requires sufficient cell density in the region over the flight deck to maintain simulation fidelity and to prevent artificial dissipation of the turbulent energy. A mesh size of 100 million cells was required to resolve the turbulence over the deck and astern of the ship for use in

both fixed-wing and rotary-wing flight simulation. A steady atmospheric boundary layer (ABL) was applied to the full-scale CFD as an inlet condition to represent the flow over the sea surface [12, 38-39].

Figure 3 shows the vortical structures in the CFD-generated QEC airwake for a headwind, using the Q-criterion vortex identification method, as iso-surfaces coloured by instantaneous streamwise u-velocity. Also shown in Fig. 3 are the x, y, z axes relative to the ship, the origin is on the flight deck vertically above the ship's centre of gravity. The longitudinal axis, or x-axis, is parallel to the ship's centreline (positive towards the stern); y is athwartships (positive starboard); and z is in the vertical direction (positive upwards). The corresponding velocities in these axes are u, v and w, respectively. To create a continuously unsteady flow field in the flight simulation environment, 30 seconds of unsteady three-dimensional velocity components were computed and looped within the simulation to provide a sustained airwake.

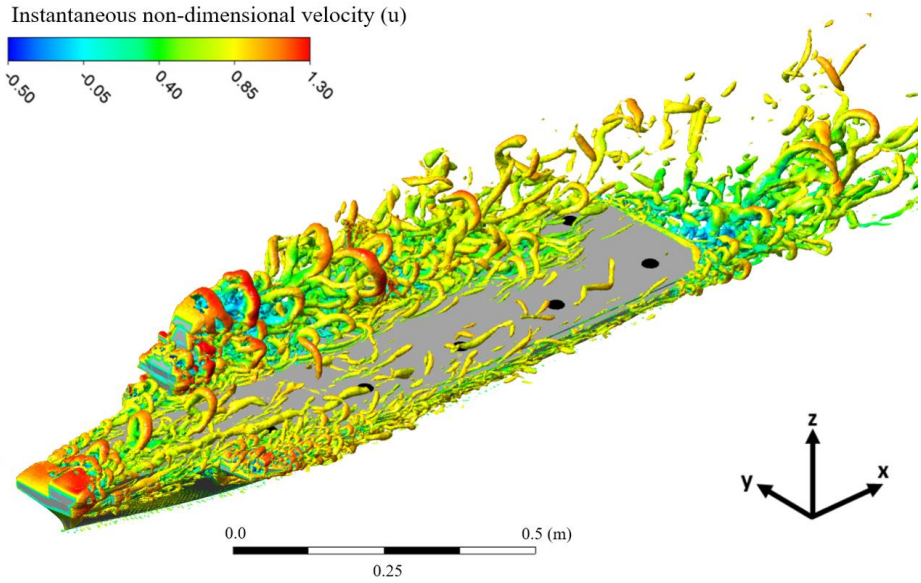

Fig. 3 Headwind flow over QEC model presented as instantaneous iso-surfaces of Q-criterion coloured by u-velocity.

Illustrations of the airwakes for the three wind conditions used in the flight trials are shown in Fig. 4. Each image shows flow over the QEC as mean streamlines coloured by turbulence intensity; the streamlines are in vertical planes passing through the deck landing spots, shown as black spots. Figure 4 also contains contours of turbulence intensity in a horizontal plane that is located 10m above the flight deck. The significance of the 10m is that this is the approximate height of the centre of gravity for rotary-wing aircraft when translating across the deck during a vertical landing, according to [40]. In the headwind case the turbulence intensity over the spots is relatively low at less than

5%, with the exception of the landing spot in the lee of the aft island which shows an increase in turbulence intensity due to the air flow shedding off the islands. In this study, turbulence intensity is expressed as a percentage of the mean freestream velocity, not the local mean velocity.

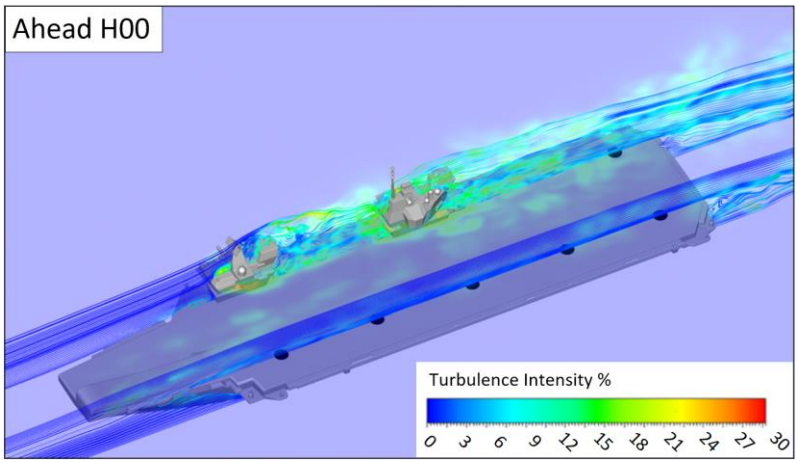

a)

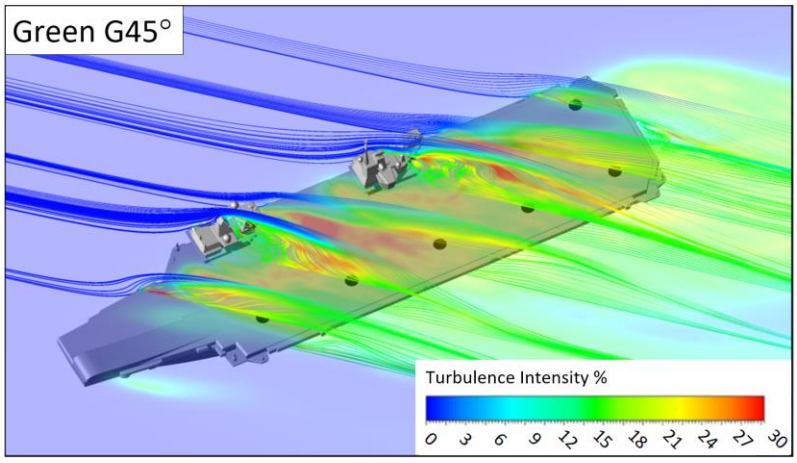

b)

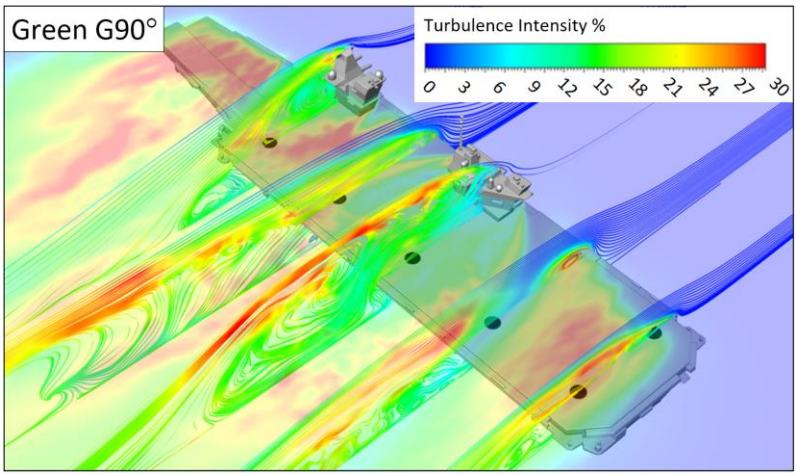

c)

Fig. 4 Illustrations of QEC airwakes for winds from Ahead (a), Green 45° (b), Green 90° (c).

While it is preferable to launch and recover aircraft to the ship in a headwind, where there will be less flow disturbance over the flight deck and higher relative air speeds, and hence improved lift for the aircraft, there will inevitably be times when the relative wind will be from directions other than ahead. It is important, therefore, to have an understanding of the air flow over the deck for all wind directions, e.g. [41-42]. Taking the three images in Fig. 4 together, it can be seen that as the wind moves from ahead to abeam, so the turbulent flow from the islands encroaches on more landing spots, it becomes more turbulent at each landing spot, and more turbulent off the port-side affecting helicopter landing approaches; areas in the flow with turbulence levels of up to 30% can be seen. It can be expected, therefore, that winds from starboard, i.e. Green winds, will increase pilot workload during vertical landings at each spot, an observation that is generally consistent with operational experience for aircraft carriers with the superstructure situated on the starboard side of the flight deck. (Winds from the port side of a ship are known as Red winds). Of particular interest to this paper are spots 5 and 6, which are the two nearest to the stern; spot 6 being situated behind the island. The significance of these two spots is that they have been initially designated as primary landing spots for rotorcraft. Therefore, because of the challenges to the aircraft from Green winds, and the designation of spots 5 and 6 to helicopter operations, the simulated trials reported in this paper will concentrate on these winds and spot locations. Figure 4 (a) shows that the turbulence intensity level over each spot in an ahead wind is low with a small increase to approximately 10% at spot 6 due to the presence of the aft island in the freestream flow. As the wind approaches from 45° off the starboard side, the turbulence intensity increases at spot 5 and 6 to close to 20% as shown in Fig. 4 (b). A further increase in turbulence intensity, to about 25%, can be seen in Fig. 4 (c) over spot 5 in a Green 90° wind; however, the flow around a hover position above spot 6 shows a turbulence intensity of less than 5% which increases as the height above the deck decreases.

The CFD method used to create the unsteady airwakes was validated by comparing the solution to experimental mean and turbulent velocity components measured in the flow over a 1:200 physical model of the ship submerged in a water tunnel. Comprehensive experimental data and greater detail of both the experiment and the CFD methodology can be found in [34-35]. However, to demonstrate the good agreement between the CFD (red-line) and the experimental data (black-line) reported in [34], Fig. 5 shows a comparison of the mean streamwise u-velocities along vertical lines at various positions over and astern of the ship, in a vertical plane passing through the centre of the islands. The airwake is for a headwind and is illustrated by contours of turbulence intensity.

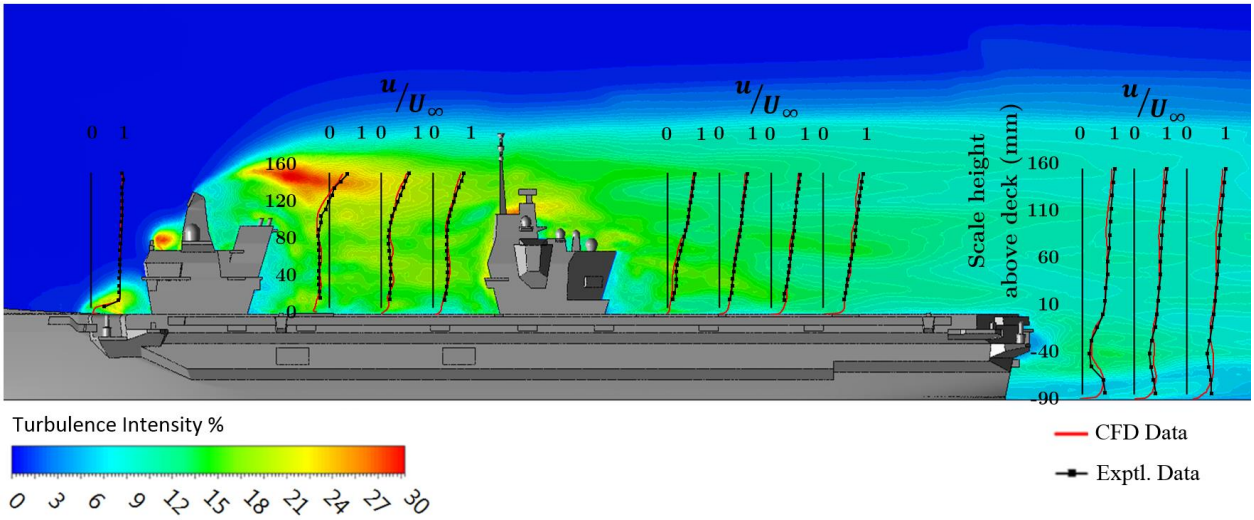

Fig. 5 Comparison of experiment and CFD mean u-velocity in plane through centre of islands.

B. Airwake interpolation and integration with FLIGHTLAB

The purpose of the simulated flight trial was to evaluate the helicopter handling qualities and pilot workload when recovering to the QEC for three different wind directions: Ahead, Green 45° and Green 90°. The wind speeds and direction relative to the ship are known as the Wind Over Deck (WOD). As seen earlier in Fig. 4, the Green winds will create turbulent air flow and should present the pilot with challenging conditions. It was originally intended to use the same wind speeds at each wind angle; however, it was found during the trials that the Green winds presented a particular challenge to the pilot, so lower wind speeds were tested for the Green 45° and 90° conditions, as listed in Table 1.

Table 1 Test Conditions.

Azimuth (WOD)	Wind Speed (WOD), kts
Ahead	25, 35, 45
Green 45°	15, 25
Green 90°	15, 25, 35

Figure 6 schematically illustrates the process for integrating the computed unsteady velocity components of the airwake with the FLIGHTLAB SH-60B helicopter flight dynamics model. Thirty seconds of unsteady airwake was computed for each wind direction at 100Hz on an unstructured grid. The three-dimensional velocity components were

then interpolated onto a smaller structured grid and down-sampled to 25Hz. The structured grid is shown in Fig. 6 with dimensions 300m in length by 150m in width by 24m in height and a grid spacing of 1m; all flying operations where constrained to take place within this rectangular volume. Airwakes were computed at each wind angle with a wind speed of 30kts. The Strouhal number relates the distinct frequencies of vortices shed from the ship superstructure with the flow speed and the characteristic length of the ship. As the ship is regarded as a bluff body and the Reynolds number is high, the Strouhal relation is used to scale the airwake frequency to a required flow speed. The validity of Strouhal scaling of ship airwakes was demonstrated in [43], and was used in this paper to obtain airwakes at relative wind speeds of 15kts to 45kts.

The CFD-computed ship's airwake is integrated into the aircraft's flight dynamics model using Simulink. The velocity data for each WOD condition is converted into a series of lookup tables and applied to the helicopter flight dynamics model at Aerodynamic Computation Points (ACPs) in real time within the FLIGHTAB software as the pilot manoeuvres the aircraft within the airwake; as the aircraft has no effect on the airwake this is integration known as one-way coupling. The distribution of ACPs on the SH-60B model can be seen in the upper right of Fig. 6. Ten ACPs are distributed along each of the four main rotor blades, one at the fuselage centre of gravity, one on each of the port and starboard stabilisers, two on the vertical tail, and a final ACP at the centre of the tail rotor hub, giving a total of 46 ACPs. Although two-way coupling has been achieved for a helicopter fixed in a hover position over a ship's flight deck [44], it is not currently feasible to compute the solution in real-time for flight simulation, particularly for the large cell count required by the large flight deck of the QEC aircraft carrier [45].

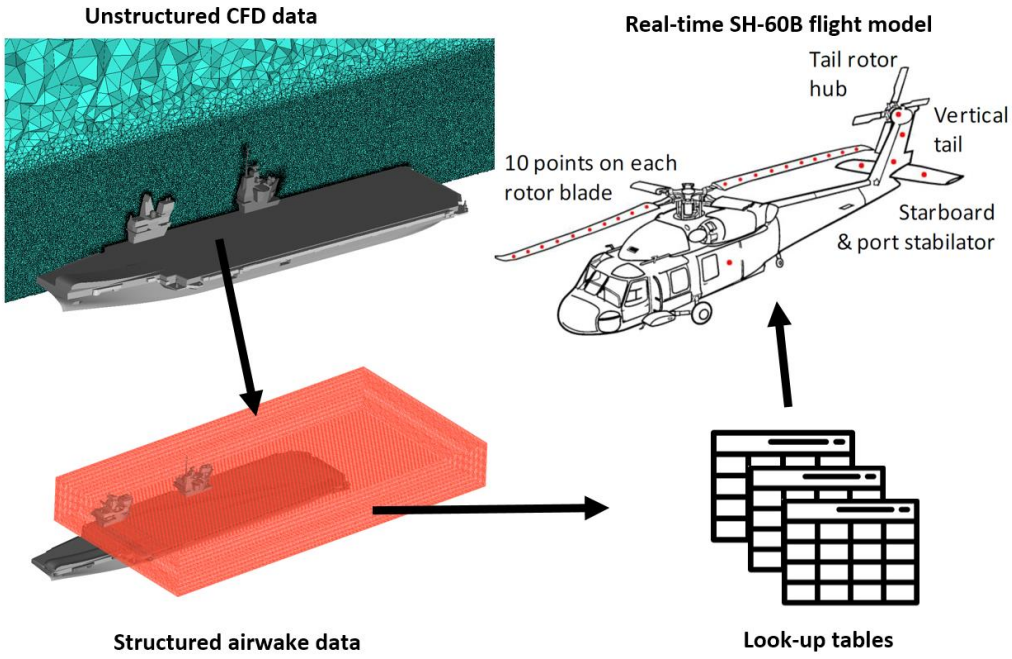

Fig. 6 Integration of CFD airwake with helicopter flight dynamics model.

C. Ship Motion

Pilots use the ship's superstructure and deck to obtain visual cues when flying close to the ship, so realistic ship motion is required. A hull form and appendages representative of a generic 280m long warship was used with the ship motion software, ShipMo3D, a well-validated ship motion potential-flow code developed at Defence Research and Development Canada (DRDC) – Atlantic [46] and made available to UoL. Ship motion was calculated in sway, surge and heave, and in pitch roll and yaw for waves coming from ahead and starboard. Sea states were defined using the Bretschneider Spectrum. Sea state 4 was used for the lower wind speeds and sea state 5 for the higher wind speeds; a typical ship speed through the seaway of 12kts was applied.

Figure 7 shows deck motion data in heave (vertical), roll and pitch computed for spot 5 in sea state 5 for waves from ahead and 45° from starboard, i.e. Green 45°; spot 6 will have similar displacements. As expected, the greater motions are stimulated by the oblique waves. Heave motion, augmented by deck pitch and roll at spots away from the centre of rotation, is the most important motion for the pilot attempting to land to the deck and, as can be seen in Fig. 7 the vertical displacement at the landing spot was not excessive and mostly less than 2m. As will be seen in the flight test results later in the paper, the test pilot did not identify deck motion as a factor contributing to workload during a deck landing.

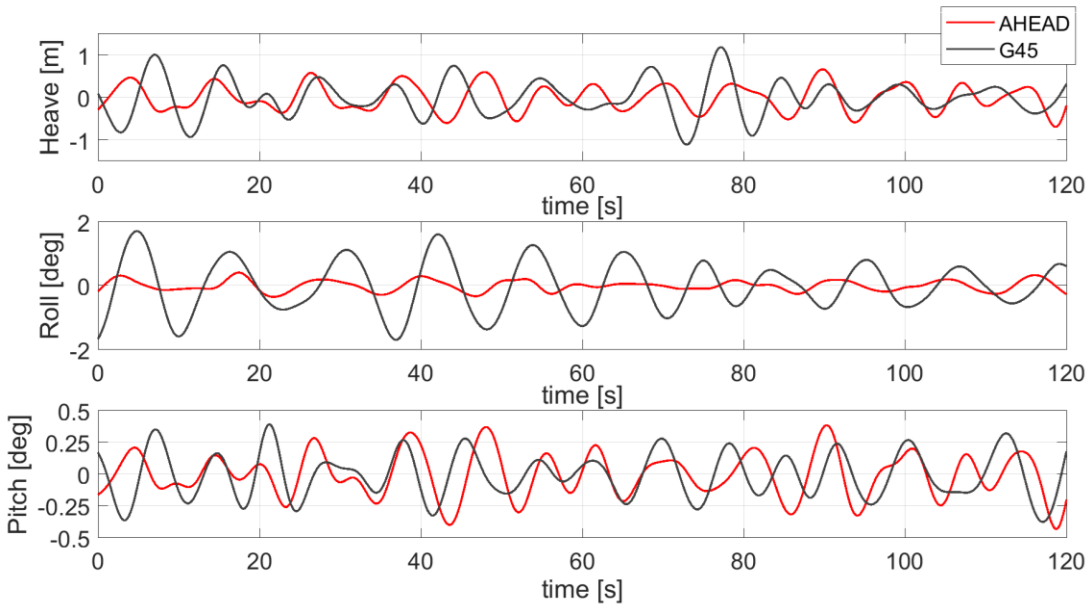

Fig. 7 Computed ship motion at landing spot 5 for waves from Ahead and Green 45° in sea-state 5.

D. Flight Test Procedure

During the simulated flight trial, a highly experienced former Royal Navy (RN) helicopter test pilot was instructed to land at spots 5 and 6 in the eight WOD conditions at the wind speeds shown in Table 1. The pilot performed the standard UK port-side forward-facing recovery technique, which requires the pilot to guide the helicopter to a hover position off the port side of the ship, matching the ship's speed, followed by a lateral translation across the deck to hover over the landing spot, before descending to land on the flight deck. Each landing was split into three Mission Task Elements (MTE), illustrated in Fig. 8. The first is the lateral traverse across the deck from the port side of the ship to a hover position over the landing spot. The second MTE requires the pilot to maintain the hover position for 30 seconds in preparation for landing and, finally, the third MTE is the descent from the hover position to touch down on the flight deck. The standard UK port-side forward-facing approach was used for each landing spot to maintain consistency. The difficulty of the landing task was assessed by the test pilot using two subjective rating scales: a workload was assigned to each MTE from the Bedford workload rating scale, and a rating from the DIPES was given for the overall landing task. The two scales are shown in Fig. 9 and Fig. 10 respectively.

Fig. 8 Mission task elements on recovery to QEC landing spots 5 (left) and 6 (right).

The Bedford workload rating scale assesses the pilot's perceived workload and is based on the pilot's spare capacity when performing a task, where workload is defined as the integrated physical and mental effort generated by the perceived demands of a specified piloting task [47]. As shown in Fig. 9, the Bedford workload scale has 10 ratings awarded by the pilot, based on an evaluation of their spare capacity during the set task. A rating of 1-3 indicates that workload was satisfactory during the task. Ratings of 4-6 are awarded where the workload for a task was not satisfactory, reducing the pilot's capacity to perform ancillary tasks such as radio communication, while ratings of 7-9 are awarded where the task can be performed, yet the workload is deemed intolerable. Finally, a rating of 10 is awarded in situations where the pilot is unable to complete the task due to high workload, and so must abandon the task.

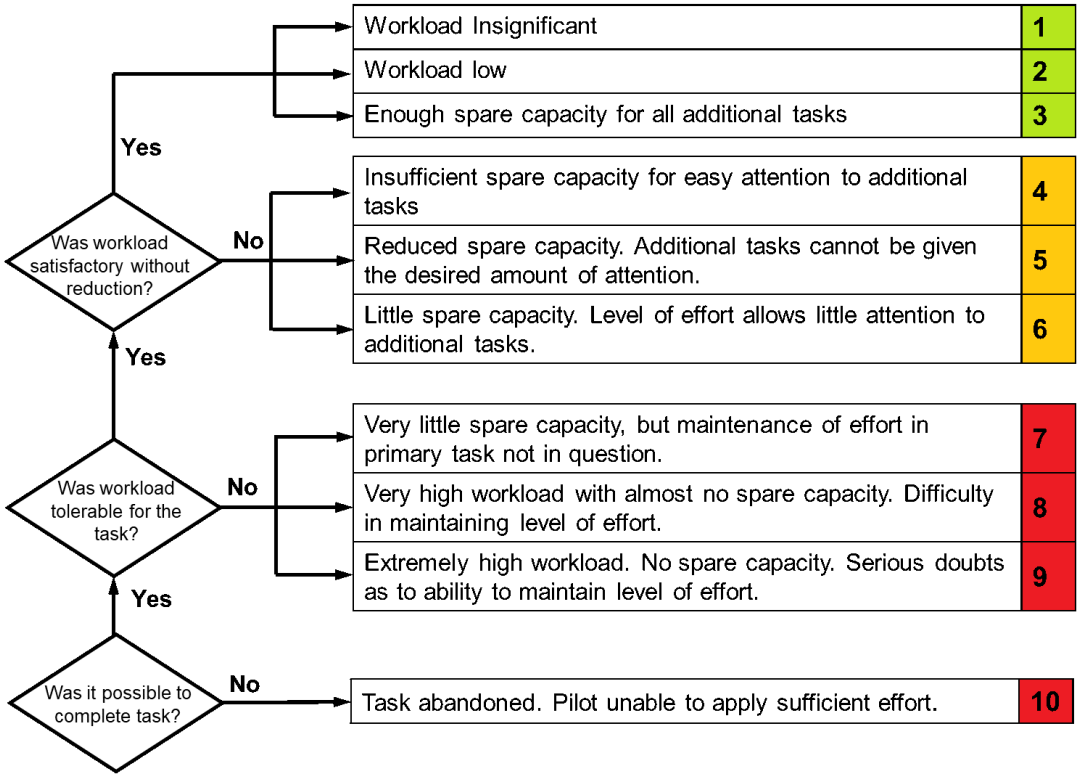

Fig. 9 Bedford workload rating scale [47].

The DIPES assesses the overall landing task and is widely used by NATO member countries to determine limiting conditions for ship-helicopter combinations. DIPES differs from the Bedford scale in that it is a coarser scale which also accounts for aircraft physical control activity and identifies environmental factors such as deck motion and turbulence [30]; DIPES is therefore particularly suited for qualification testing where, although pilot workload may be low, control limits can be encountered. The DIPES chart shown in Fig. 10 can be used to give a rating of 1-5 for a launch/recovery task. A rating of 1-3 ranks effort from slight to the highest tolerable while still being considered within acceptable bounds and within the capabilities of an average fleet pilot. A rating of 4 is deemed to be unacceptable on the basis that an average fleet pilot would not be able to complete the task in a consistently safe manner. A rating of 5 indicates that the task cannot be safely completed by fully proficient crews even under controlled test conditions. Beneath the DIPES scale is a list of suffixes the pilot may assign to a given rating to specify the causes of the workload.

EFFORT	GUIDANCE	DIPES
Slight to Moderate	Reasonable compensation required. Tracking and positioning accuracy is consistently maintained throughout the operation. Fleet pilots will have enough spare capacity to conduct ancillary tasks.	**1**
Considerable	Significant compensation required. Tracking and positioning accuracy occasionally degrades during peaks in ship motion, sea spray or turbulence. Fleet pilots will have difficulty conducting ancillary tasks.	**2**
Highest Tolerable	Highest tolerable compensation required. Tracking and positioning accuracy degrades regularly during peaks in ship motion, sea spray or turbulence. Fleet pilots will be able to keep up with task requirements but no more. Degraded operations (ship or aircraft) will probably require an abort. Repeated safe operations are achievable. This point defines the recommended limit.	**3**
Excessive	Excessive compensation required. Accuracy is poor in one or more axes. Fleet pilots will be purely reacting to external influences rather than anticipating them. A safe abort may not be possible if an aircraft or ship system is lost during a critical phase of the evolution. Fleet pilots under operational conditions could not consistently repeat these evolutions safely.	**4**
Dangerous	Extreme compensation required. Repeated safe evolutions are not possible even under controlled test conditions with fully proficient crews.	**5**

Acceptable DIPES 1-3	Unacceptable DIPES 4-5

Note: Each DIPES rating may be given one or more suffixes to describe the cause(s) of the increased workload.

Pitch control:	P	Height control:	H
Turbulence:	T	Spray:	S
Roll control:	R	F/Aft positioning:	F
Deck motion:	D	Torque control:	Q
Yaw control:	Y	Lateral positioning:	L
Visual cues:	V	Funnel exhaust:	E
A/C attitude	A		

Fig. 10 DIPES rating scale [30].

During the simulated flight trials, the pilot awarded Bedford workload ratings for each MTE, along with a DIPES rating for the total recovery to the ship; the pilot's comments were also documented for further analysis. In addition, flight test data was recorded providing time-domain information for pilot input to the cyclic, collective and pedal controls, as well as aircraft position, attitude and accelerations in six degree of freedom. The airwake velocity components at each of the 46 ACPs were also recorded.

III. Flight Trial Results

A selection of results from the flight trials are presented and discussed in the following sections. The results have been collated as tables of pilot ratings, and figures showing pilot control activity and aircraft position for both the overall landing task, and for the 30 second hover over the landing spot.

A. Pilot Ratings for Deck Landing Task

1. Ahead

Figure 11 presents the Bedford Workload ratings for each MTE and the overall DIPES ratings when landing to spots 5 and 6 in winds from ahead at speeds of 25kts, 35kts and 45kts. The pilot gave workload ratings of 1 to 3 for each task in an Ahead wind indicating that the workload was satisfactory; a maximum DIPES rating of 2 in an Ahead wind was given during landing to spot 6 in winds of 35kts and above.

QEC AHEAD						
			Bedford Workload ratings			
Spot	DIPES suffixes	Wind	MTE 1	MTE 2	MTE 3	DIPES
5		25kts	1	2	2	1
		35kts	1	2	2	1
		45kts	1	2	2	1
6		25kts	1	2	2	1
		35kts	1	3	3	2
		45kts	1	3	3	2

Fig. 11 Bedford Workload and DIPES ratings in Ahead WOD.

2. Green 45°

Figure 12 presents the Bedford Workload ratings for each MTE and the overall DIPES ratings when landing to spots 5 and 6 at speeds of 15kts and 25kts in a Green 45° WOD. After experiencing difficult flying conditions in the 25kts wind, the pilot elected not to fly at a higher wind speed; an outcome that would correspond with establishing the operational limit during a real trial.

QEC Green 45°						
			Bedford Workload ratings			
Spot	DIPES suffixes	Wind	MTE 1	MTE 2	MTE 3	DIPES
5	Y,H,T,F,L	15kts	4	4	4	2
	Y,H,T,F,L	25kts	5	6	6	3
6	Y,H,T,F,L,V	15kts	4	5	4	3
	Y,H,T,F,L,V,Q	25kts	5	7	8	4

Fig. 12 Bedford Workload and DIPES ratings in a Green 45° WOD.

All of the landing tasks in a Green 45° wind condition showed less than satisfactory workload conditions. Winds higher than 25kts on landing to spot 6 caused intolerable workload for the pilot; this is reflected in a DIPES rating which exhibits excessive compensation required. Common causes of each DIPES rating given by the pilot in a Green 45° were as follows: Yaw control (Y), Height control (H), Turbulence (T), Forward/Aft positioning (F) and Lateral positioning (L).

3. Green 90°

Figure 13 presents the Bedford workload ratings for each MTE and the overall DIPES ratings when landing to spots 5 and 6 at speeds ranging from 15kts to 35kts in a Green 90° WOD, i.e. a beam wind. During the port-side forward-facing landing manoeuvre, the 90° wind presents a side wind to the helicopter thus requiring increased pedal and lateral cyclic inputs. While the pilot did elect to land to spot 6 for a 35kts wind, he did not do so for spot 5 due to the challenging conditions experience at 25kts.

QEC Green 90°						
			Bedford Workload ratings			
Spot	DIPES suffixes	Wind	MTE 1	MTE 2	MTE 3	DIPES
5		15kts	1	3	3	2
	Y,T,F,L	25kts	3	4	4	4
6	Y,F	15kts	1	3	4	2
	Y,T,F,L,P	25kts	3	4	5	4
	Y,T,F,L,P,V,A	35kts	9	8	8	5

Fig. 13 Bedford Workload and DIPES ratings in a Green 90° WOD.

The workload ratings for each task in a Green 90° condition for both landing spots shown in Fig. 13 increase with wind strength. Helicopter recovery was conducted to spot 6 in a 35kts wind that would not have been attempted in a

real FOCFT due to the large workload observed during the previous 25kts; the recovery was attempted to observe the effects of operating in extreme workload conditions.

B. Aircraft Position During Deck Landing Task

Figures 14 to 16 show the helicopter's lateral, longitudinal and vertical position over the deck whilst recovering to the ship in the three WOD conditions. The position is recorded at the aircraft's centre of gravity.

1. Ahead

In the Ahead WOD condition shown in Fig. 14 the pilot was able to maintain a desired vertical height while translating across the edge of the deck to the hover position over landing spots 5 and 6. As the wind speed was increased from 25kts to 45kts the vertical position during the translation was similar. After the longer translation to spot 6, the aircraft had a longitudinal position which the pilot corrected by moving forward when in line with the landing spot; the longitudinal drift was greater in the stronger 45kts wind.

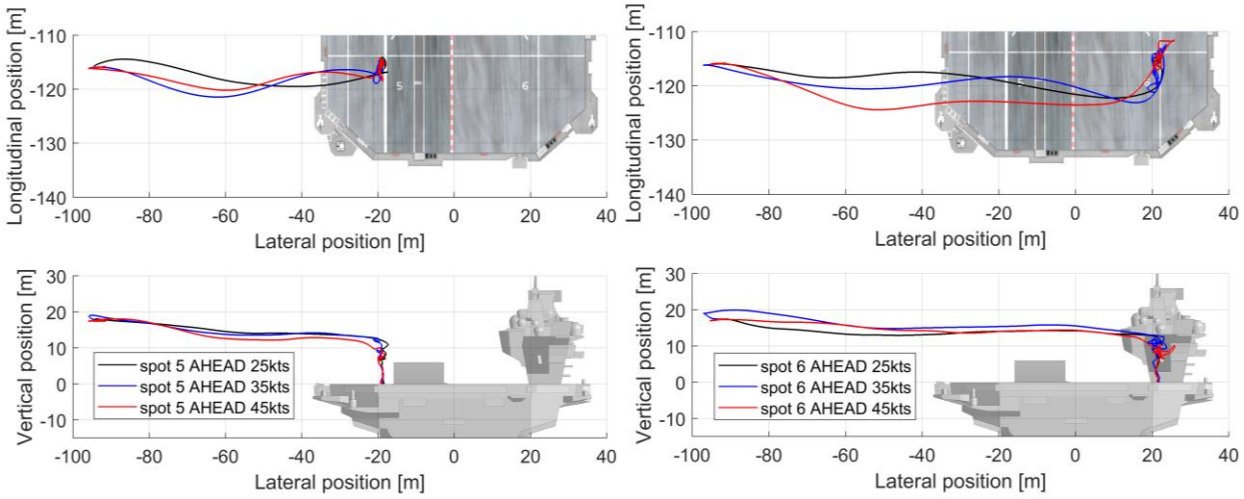

(a) **(b)**

Fig. 14 Helicopter position in an Ahead wind at spots 5 (a) and 6 (b).

2. Green 45°

Although the pilot was able to maintain height throughout the translation in a 15kts Green 45° WOD condition as shown in Fig. 15, increasing the wind speed to 25kts resulted in more flight path disturbances. The pilot was also

required to correct the longitudinal drift and move the aircraft forward after the lateral translation to position over landing spot 6.

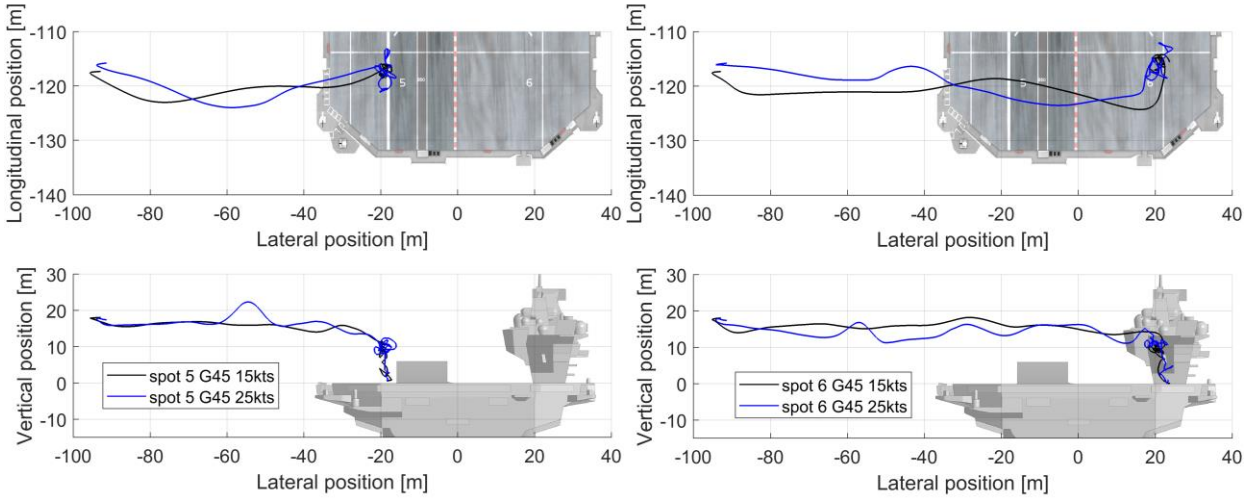

(a) **(b)**

Fig. 15 Helicopter position in a Green 45° wind at spots 5 (a) and 6 (b).

3. Green 90°

Figure 16 shows the aircraft's position during recovery in a Green 90° WOD. Although the aircraft's vertical position was less disturbed while translating across the deck compared with the Green 45° WOD, the pilot was unable to maintain a precise longitudinal position during the traverse manoeuvre for the greater distance to spot 6.

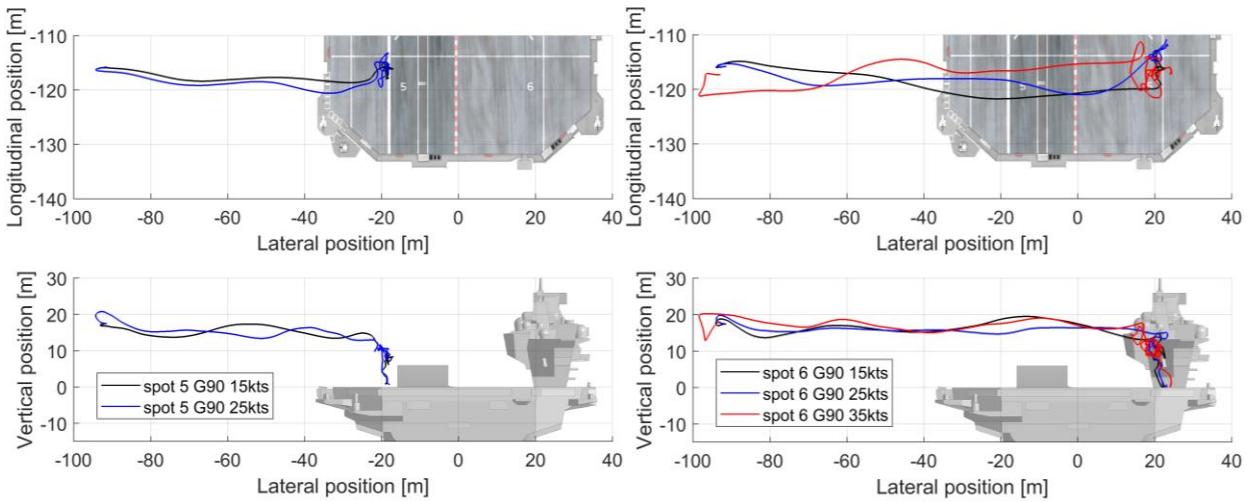

(a) **(b)**

Fig. 16 Helicopter position in a Green 90° wind at spots 5 (a) and 6 (b).

C. Torque and Collective Control During the Landing Task

Although it is recognised that the aircraft controls are coupled, they have been presented separately to more easily compare the effect of the different WOD conditions at each spot location. Figures 17 to 19 show the pilot's torque and collective inputs during recovery to the ship for each WOD condition at spot 6. Data for spot 5, which has a shorter translation, has been omitted for the sake of brevity. In the figures the time histories are split by vertical dashed lines to show the three MTE's: lateral translation, hover and touchdown. The red horizontal dashed line indicates the 100% torque limit.

1. Ahead

The collective and torque inputs during aircraft recovery to the ship in an Ahead WOD at spot 6, Fig. 17, shows that there was relatively little activity, although there is an increase in activity at the higher wind speeds.

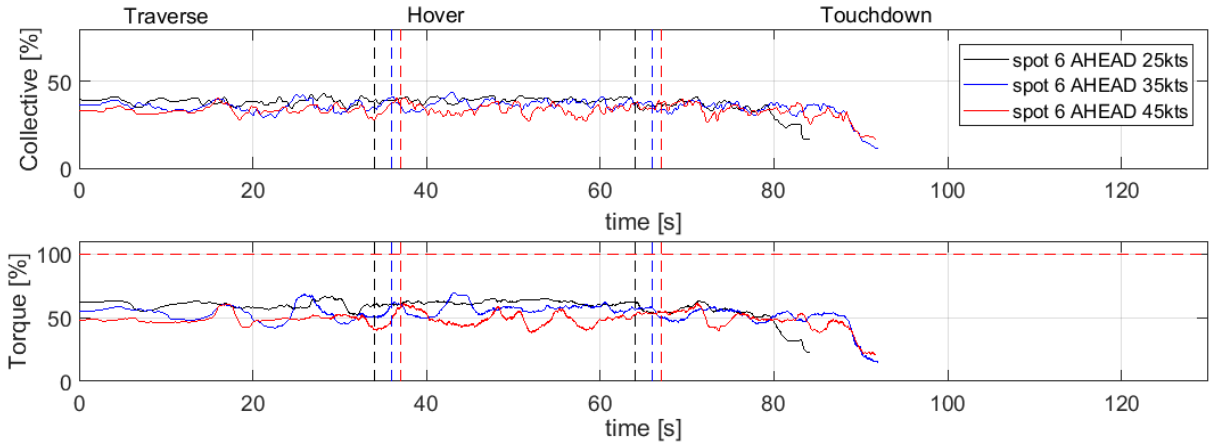

Fig. 17 Collective and Torque inputs in an Ahead wind at spot 6.

2. Green 45°

During recovery to spot 6 in a Green 45° WOD, much greater activity is observed in the pilot's collective and torque inputs for both wind speeds compared with winds from Ahead, as can be seen in Fig. 18.

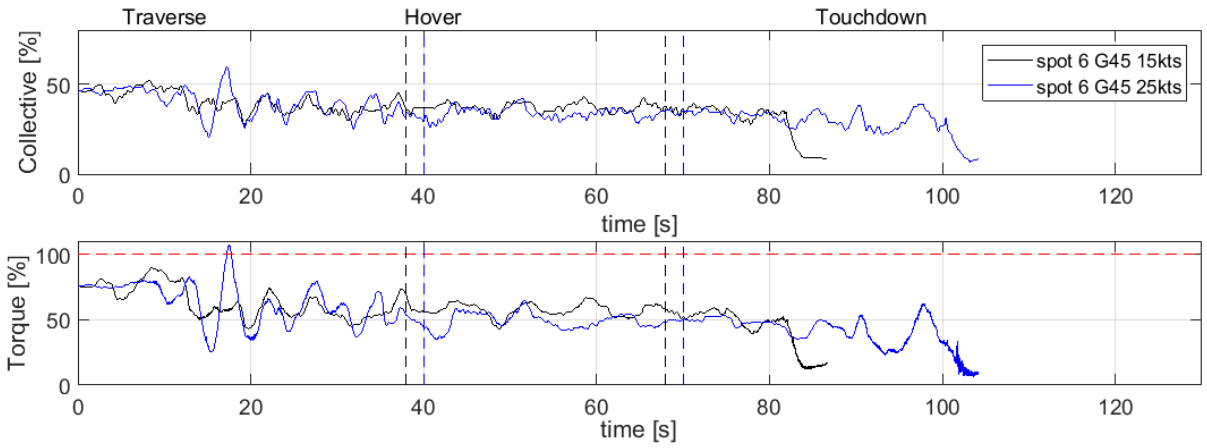

Fig. 18 Collective and Torque inputs in a Green 45° wind at spot 6.

3. Green 90°

Figure 19 shows that the pilot's control activity in collective and torque during the landing task in the Green 90° winds were lower than those seen in the Green 45° winds. It is also noticeable that in the 45kts wind the overall landing task, particularly MTEs 1 and 3, the translation and landing, took significantly longer with the pilot spending about one minute on MTE 1, a clear indicator of high workload.

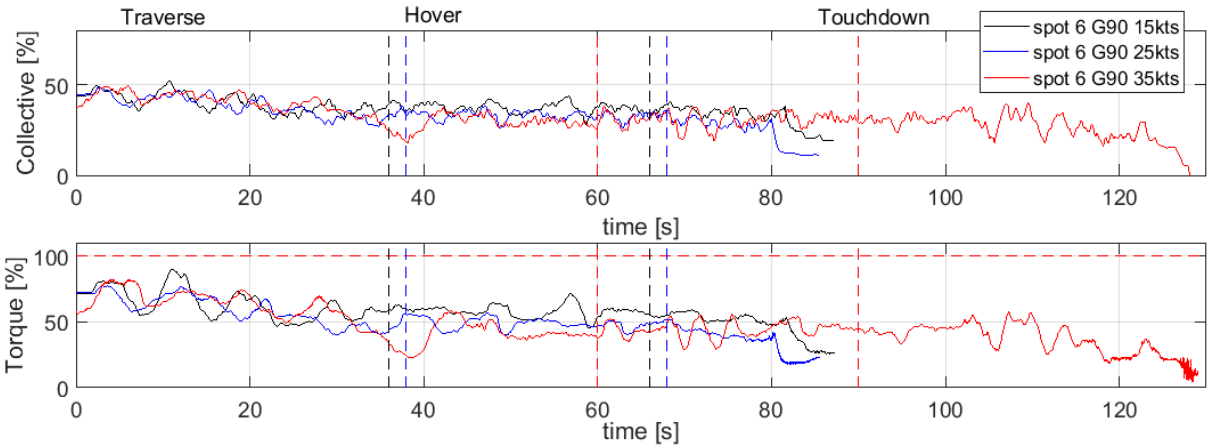

Fig. 19 Collective and Torque inputs in a Green 90° wind at spot 6.

D. Pedal Inputs During Landing Task

During the simulated flight tests the pilot commented several times during recoveries in the Green 45° and Green 90° WOD conditions that the pedal limits had been reached. Figures 20 to 22 show the pedal control inputs for each WOD condition; full right and left pedal are given as 50% and -50% respectively with the 10% pedal margins shown as horizontal dashed red lines.

1. Ahead

Figure 20 shows the limited pedal input on landing to spot 5 for 25kts, 35kts and 45kts winds; increased activity is shown when landing at spot 6. Pedal activity is well within the pedal margins.

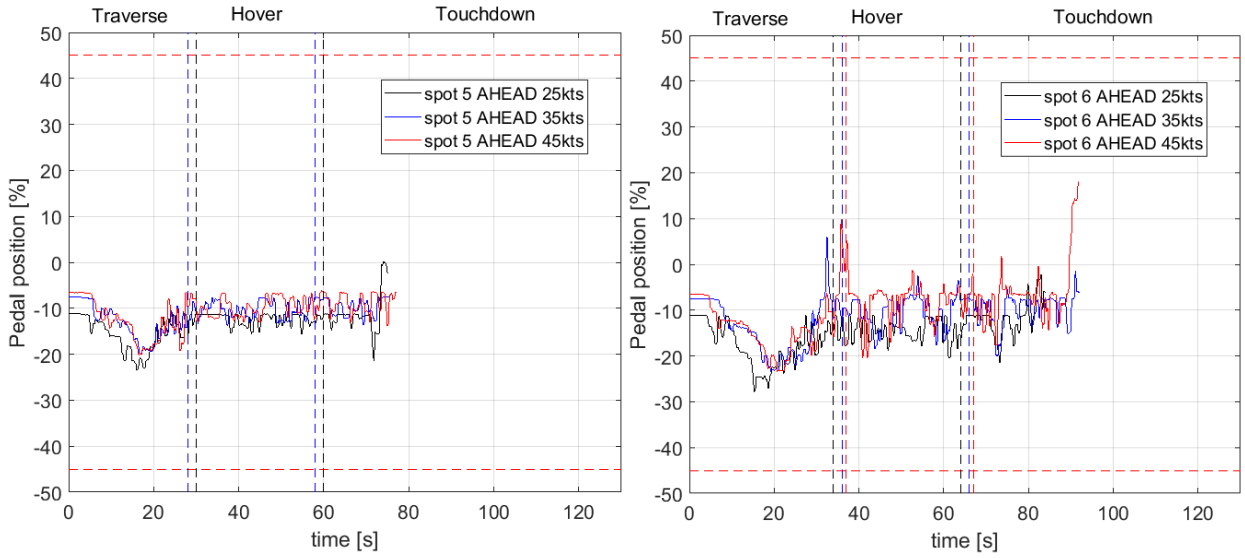

(a) **(b)**

Fig. 20 Pedal position in an Ahead wind at spots 5 (a) and 6 (b).

2. Green 45°

The pedal input time histories on landing to spots 5 and 6 in a Green 45° WOD are shown in Fig. 21. An increase in control activity can be seen compared with the headwind. Also, the control activity in the 25kts wind was greater than in the 15kts wind for both spots. As well as the control activity and greater excursions in the pedal controls, it can be seen that a significant left pedal input was applied for the majority of the mission to overcome the crosswind component in the 45° wind.

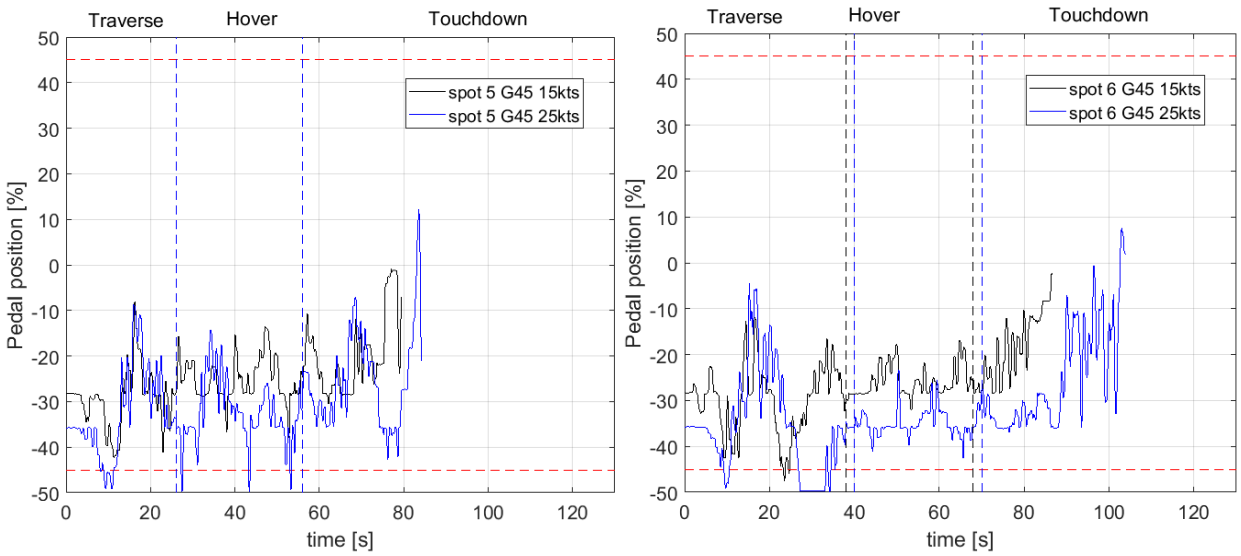

(a) **(b)**

Fig. 21 Pedal position in a Green 45° wind at spots 5 (a) and 6 (b).

3. Green 90°

Figure 22 shows the pilot's pedal control inputs for a Green 90° WOD. As for the winds from Green 45°, an increase in the wind speed required the pilot to maintain a greater pedal input. The amplitude of pedal inputs on landing to both spots was less than that for the Green 45° WOD. Similarly, to the control activity exhibited in a Green 45°, the pedal 10% margin was infringed several times in the Green 90° but for longer periods; at spot 6 in a 35kts wind full left pedal was employed for much of the manoeuvre.

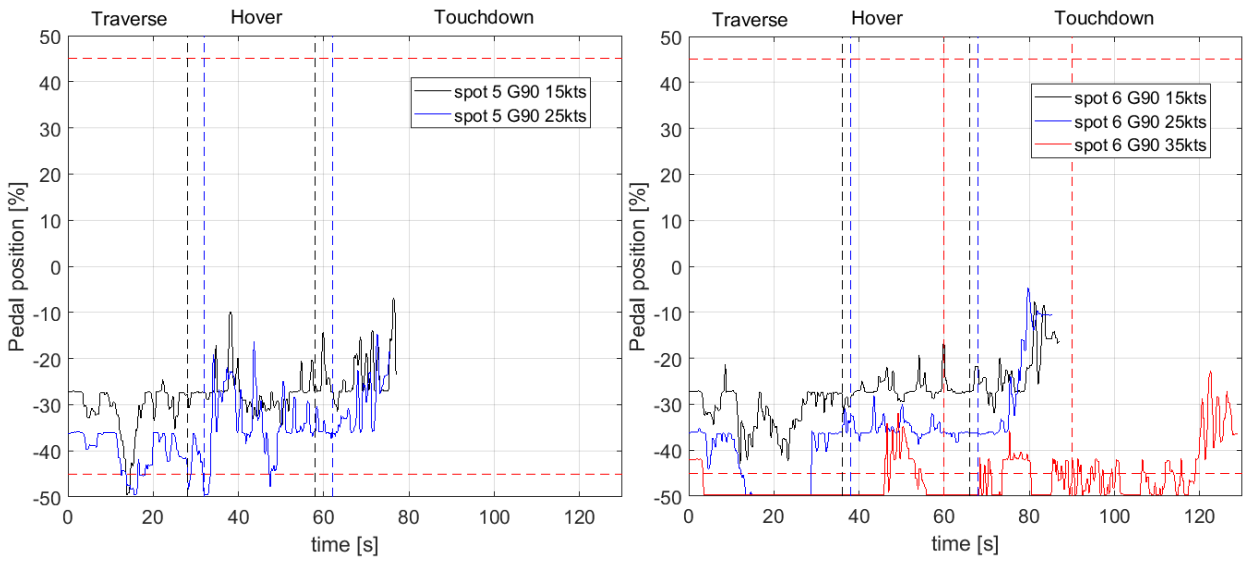

(a) **(b)**

Fig. 22 Pedal position in a Green 90° wind at spots 5 (a) and 6 (b).

E. Aircraft Position During Hover Task and Touchdown

The lateral and longitudinal position of the aircraft's centre of gravity during the hover and touchdown MTEs is shown in Figs. 23 to 25 for each WOD condition, they are a close-up of the congested final phase of the helicopter's positional scatter over the landing spot shown earlier in Figs. 14 to 16. In Figs. 23 to 25 a solid line is used to denote the position of the aircraft's centre of gravity during the hover MTE and a dotted line is used to show the position of the aircraft's centre of gravity during the touchdown MTE. The landing spots are marked on the ship's deck as the intersection of lines running fore-aft and port/starboard, as can be seen in Fig. 8, and close-up in Figs. 23 to 25. Fore/aft lines for spots 5 and 6 are, respectively, at -18m and +22m, where the zero is the ship's centreline. The port/starboard line through both spots is -114m, measured from the ship's centre of gravity. The pilot lines up his head with these lines, but once in the hover position the spot cannot be seen. It should also be noted that the pilot sits about 3m in front of the helicopter's centre of gravity. Hence there is some variation in the aircraft's touchdown position especially in the turbulent air flow, as would be expected for rotary-wing aircraft.

Recommended limits for the amount of scatter during helicopter operations to single-spot and multi-spot RN ships are given in [48]. The deviation of the helicopter from the optimum flight path whilst positioning for landing or departing after take-off, known as airborne scatter, is determined by the rotor diameter of the helicopter. As the SH-

60B aircraft has a rotor diameter over 15.01m, and is operating to a multi-spot ship, the omnidirectional limit for airborne scatter is 3.5m; this is shown in Figs. 23 to 25 as a solid green circle centred at the aircraft's centre of gravity relative to the pilot's seated position over the landing spot.

Similarly, the landing scatter is determined by the helicopter's Maximum All Up Mass (MAUM) and defined as the deviation of the helicopter from the optimum flight path during the vertical phase of flight, which includes the descent manoeuvre post-hover during landing and climb manoeuvre pre-hover during take-off. The SH-60B operating to a multi-spot ship, having a MAUM in excess of 5400kg, gives a landing scatter limit of 2.4m; this is shown in Figs. 23 to 25 as a dashed green circle centred at the aircraft's centre of gravity relative to the pilot's seated position over the landing spot.

1. Ahead

Figure 23 shows the aircraft's position in an Ahead WOD. Over spots 5 and 6 at 25kts there was little deviation from the chosen hover position during the 30 second task and the descent. Over spot 5, even as the WOD speed was increased to 35kts and 45kts, although there are greater deviations in the longitudinal position, the pilot was still able to maintain an accurate plan position over the deck. At spot 5 the aircraft position was in both airborne and landing scatter limits for 25kts to 45kts.

For spot 6 at the higher wind speeds, there is a greater deviation, particularly in the longitudinal axis. The large deviation in the 35kts wind was not due to excessive workload, it was a corrective positioning manoeuvre by the pilot during the hover task, moving away from the spot, gaining situational awareness and then repositioning over spot 6. At spot 6 in each wind condition the aircraft's centre of gravity position was outside RN airborne and landing limits. At 25kts the scatter is tightly clustered away from the nominal landing spot centre of gravity position possibly indicating an issue with the pilot locating the landing spot.

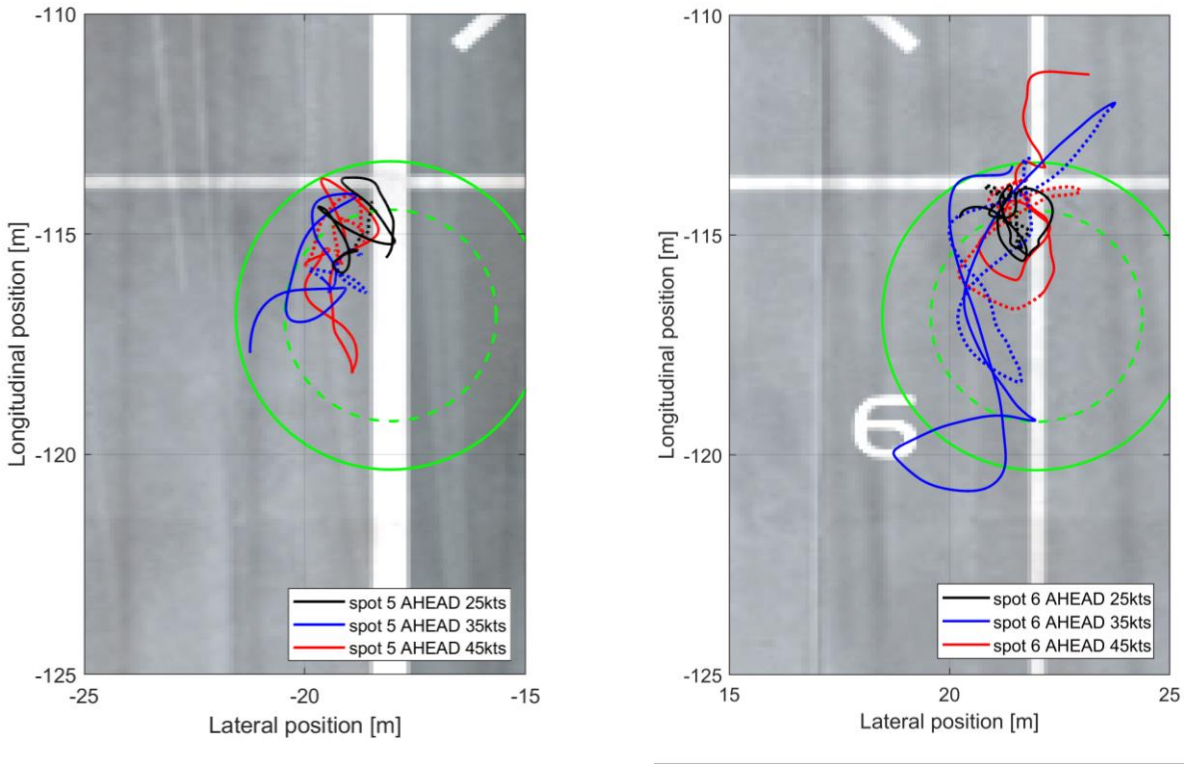

(a) **(b)**

Fig. 23 Helicopter position in hover (solid line) and descent (dotted line) in an Ahead wind at spots 5 (a) and 6 (b).

2. Green 45°

Figure 24 shows the aircraft's position during hover and touchdown MTEs over spots 5 and 6 in a Green 45° WOD. As the wind speed was increased from 15kts to 25kts, large deviations from the desired station-keeping position, both laterally and longitudinally, can be seen over both spots 5 and 6. At spot 5 in a 15kts wind the aircraft's centre of gravity was within the airborne and landing scatter limits, however, as the wind speed increased to 25kts the aircraft exceeded the limits. An increase in deviation can also be observed for spot 6 in comparison with spot 5 and the limits were exceeded for both wind speeds at spot 6.

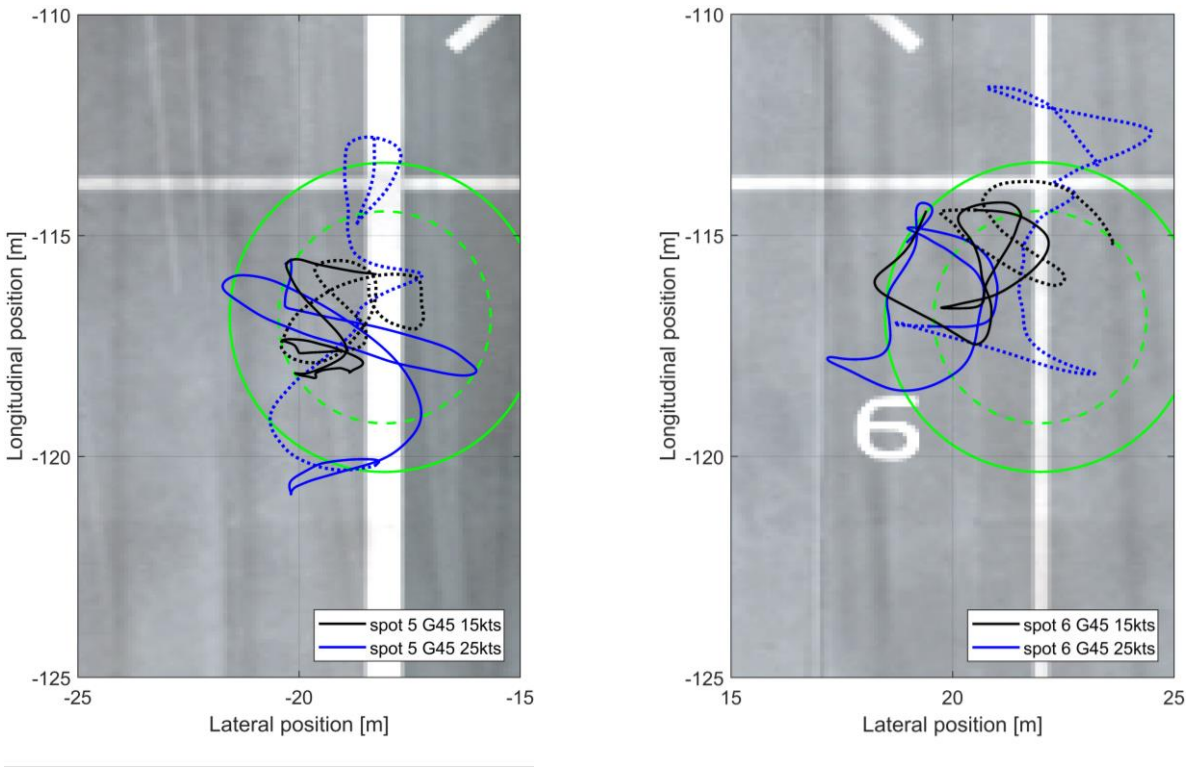

(a) **(b)**

Fig. 24 Helicopter position in hover (solid line) and descent (dotted line) in a Green 45° wind at spots 5 (a) and 6 (b).

3. Green 90°

The Green 90° WOD positions during hover and touchdown MTEs can be seen in Fig. 25. The deviations from the desired station-keeping position are smaller than seen in the Green 45° WOD, with the exception of the 35kts wind over spot 6 which, as mentioned previously, was outside of normal operational limits. Although the aircraft position was just beyond the airborne and landing scatter limits at spot 5, at spot 6 the aircraft far exceeded each scatter limit.

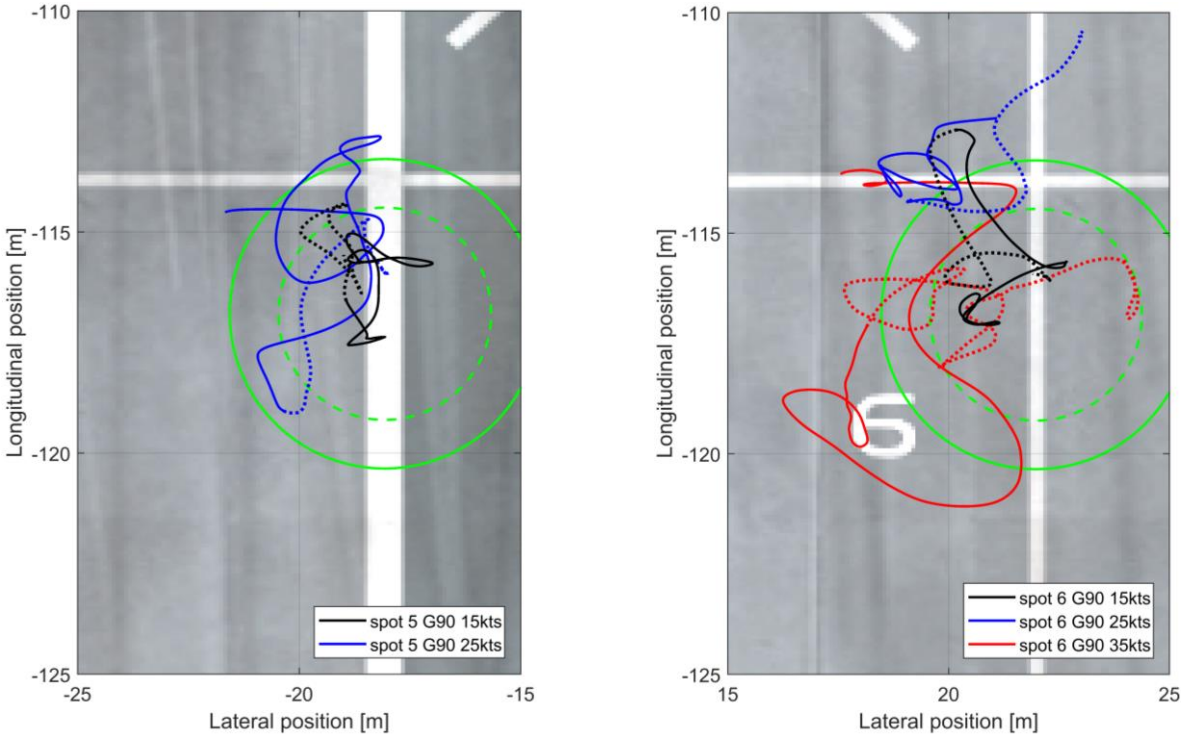

(a) **(b)**

Fig. 25 Helicopter position in hover (solid line) and descent (dotted line) in a Green 90° wind at spots 5 (a) and 6 (b).

F. Cyclic Inputs During Hover Task

Figures 26 to 28 show the pilot's cyclic control activity during the hover task, MTE 2, where the pilot was asked to hold position for 30 seconds. The central graph shows the lateral/longitudinal cyclic displacement from the trim position, while the outer time-based graphs show how the lateral and longitudinal inputs changed with time. To highlight the maximum displacements from the trim position, a broken line box has been used to bound the edge of each data set.

1. Ahead

Results are shown for the lowest and highest wind speeds of 25kts and 45kts; data for 35kts are omitted for clarity. Figure 26 shows little difference in the overall displacement of the cyclic from the trim position between spot 5 and 6

in a 25kts Ahead WOD. As the WOD speed is increased to 45kts an increase maximum displacement is seen from the trimmed cyclic position at spot 6 in comparison with spot 5.

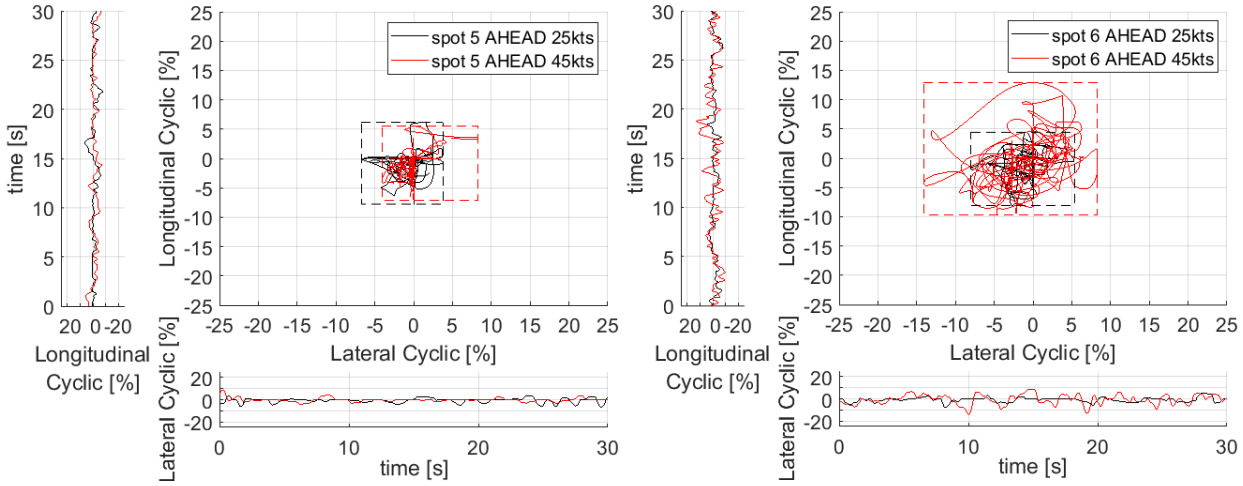

(a) **(b)**

Fig. 26 Longitudinal and lateral cyclic inputs during hover in an Ahead wind at spots 5 (a) and 6 (b).

2. Green 45°

As the WOD moved around to Green 45°, Fig. 27 shows there was a significant increase in the maximum cyclic displacements from the trim during the hover task, compared with the ahead wind. There is greater activity in the displacements for the 25kts WOD than the 15kts on landing to spot 5 and spot 6.

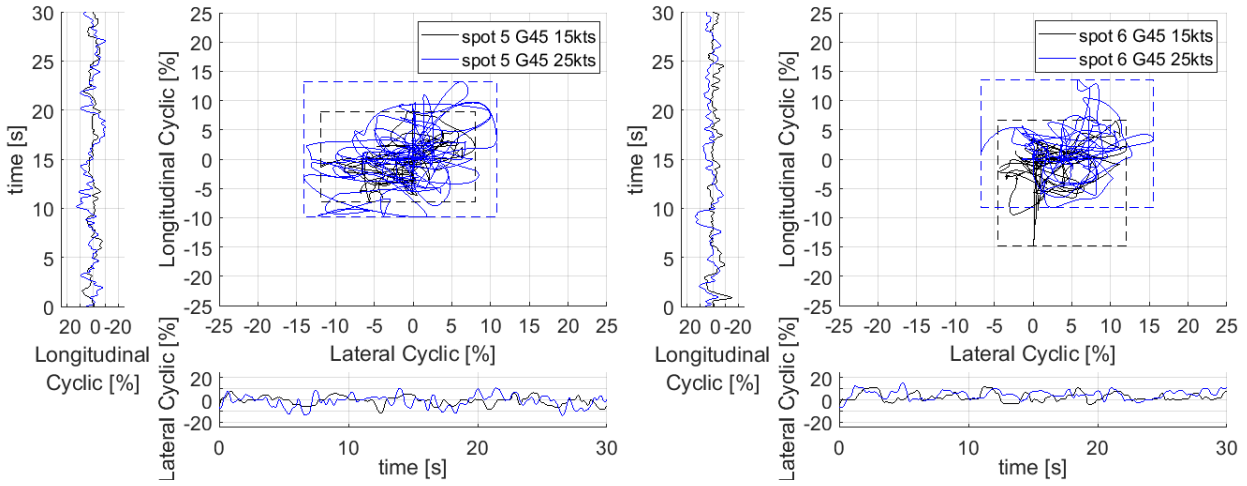

(a) **(b)**

Fig. 27 Longitudinal and lateral cyclic inputs during hover in a Green 45° wind at spots 5 (a) and 6 (b).

3. Green 90°

Figure 28 shows the cyclic inputs for 15kts and 25kts Green 90° WOD at spot 5, and at 15kts and 35kts at spot 6. An increase in the maximum displacement from the trim position can be seen for the higher wind speeds. At spot 6 in 35kts, very large deviations can be seen in cyclic activity.

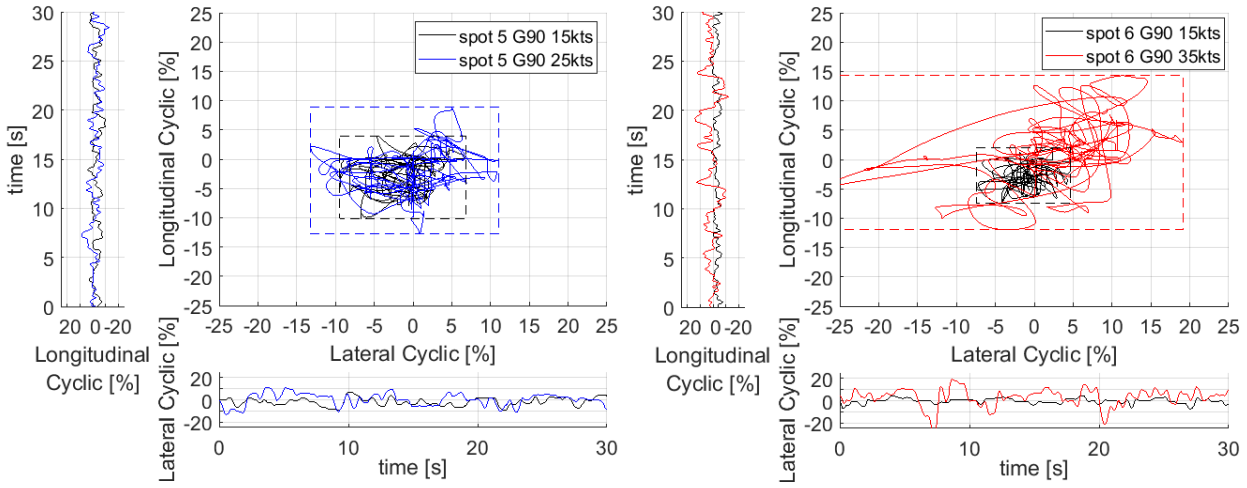

(a) **(b)**

Fig. 28 Longitudinal and lateral cyclic inputs during hover in a Green 90° wind at spots 5 (a) and 6 (b).

IV. Discussion

A. Ahead

As expected from the low turbulence levels over spot 5 shown in Fig. 4 (a) in an ahead wind, the Bedford workload for each mission task and DIPES ratings given by the pilot in Fig. 11 were relatively low. This is consistent with both the relative ease in maintaining the aircraft's position shown in Figs. 14 (a) and 23 (a) and the low level of pedal and cyclic activity by the pilot shown respectively in Figs. 20 (a) and 26 (a).

Figure 4 (a) shows spot 6 experiences higher airwake turbulence compared with spot 5, due to the aft island. Although the pilot had little to comment during the landings in an ahead wind, hence the absence of DIPES suffixes in Fig. 11, it was mentioned that at spot 6 in winds stronger than 35kts, turbulence could be felt. At 45kts landing to spot 6, the pilot noted a greater angular displacement in heading compared with the 35kts wind. The increase in Bedford workload and DIPES rating at spot 6 corresponds to larger scatter in the longitudinal and vertical positions shown in Figs. 14 (b) and 23 (b); the associated control activity to stabilise on condition with the torque, collective and pedal also increased (Figs. 17 and 20 (b)).

As the WOD speed is increased to 45kts an increase in maximum displacement is seen from the trimmed cyclic position during hover at spot 6 that is not observed when in hover over spot 5, showing the larger effect wind speed has at spot 6. The airborne and landing scatter limits described above and defined in [48] were achieved for each condition at spot 5; at spot 6 in the higher winds the limit was exceeded due the corrective positioning manoeuvres made by the pilot.

B. Green 45°

There is a significant increase in ratings for both spots in a Green 45° wind compared with an Ahead wind. In the forward-facing manoeuvre, the 45° wind presents a starboard oblique wind to the helicopter so increasing requirement for pedal input to control yaw, and lateral cyclic to overcome the side-wind component.

Referring to the CFD images in Fig. 4 (b) for Green 45°, it can be seen that neither landing spot is fully immersed in the turbulent airwake of the aft island, although turbulence from the aft vertical corner of the island will be shed across spot 5. Therefore, each spot, and the lateral translation paths, are in air flow that will not have been slowed by the blockage presented by the islands, hence the pilot's difficulty in maintaining heading. The aircraft will also

experience turbulence and steep velocity gradients due to the shear layer formed by the air shedding from the starboard edge of the deck.

On landing to spot 5 in a 15kts wind, the pilot was able to maintain low scatter during station-keeping but commented that although there was minor displacement in aircraft positioning the workload was consistent across the MTEs; the aircraft positioning is shown in Fig. 15 (a) and is reflected in the DIPES rating of 2 given by the pilot. The pilot gave several causes for this increased workload: Yaw control (Y), Height control (H), Turbulence (T), Forward/Aft positioning (F) and Lateral positioning (L).

With an increase in WOD speed from 15kts to 25kts the workload and DIPES ratings increased on landing to spot 5. The causes of the DIPES rating for the 25kts WOD were the same as for the 15kts WOD. The pilot commented that the workload was consistent throughout with random disturbances felt; the deck motion was noticed but the majority of the pilot's attention was focussed on compensating for the turbulent fluctuations. High control activity was reported with a large positional displacement, requiring considerable focus on the primary task. The difficulty in controlling the flight path and in maintaining a stable hover position, particularly in the 25kts wind, is visible in Fig. 15 (a) and, is consistent with the pilot ratings in Fig. 12 and the scatter limits in Fig. 24 (a). The pilot also noted being close to the pedal limits during the task; it can be seen from the pedal activity that in a 25kts wind, the pedal limits were exceeded momentarily several times. There was greater activity in the cyclic displacements for the 25kts WOD than the 15kts, consistent with the respective workload ratings of 4 and 6 given for hover over spot 5 in Fig. 12.

On landing to spot 6 in a 15kts wind the workload ratings in the hover (MTE 2) increased from those given for the same task in the same wind over spot 5, as did the DIPES rating. The pilot commented that the DIPES rating was awarded due to the difficulty in translating across the deck caused by the turbulence over spot 6 being noticeably higher with random hover displacement also reported. The DIPES suffixes were given due to the same causes as those over spot 5 with the addition of Visual Cues (V), due to the aft island limiting the pilot's view of a fixed horizon affecting the pilot's ability to judge the ship's motion. The pilot also reported that turbulence over spot 6 abated a little and that as the aircraft descended vertically to land the turbulence changed with a noticeable increase in turbulence around one metre above deck which will be due to the air flow separating from the landing deck horizontal edge.

With an increase of WOD from 15kts to 25kts for landings to spot 6, a large increase in workload was also experienced. Ratings in the hover and landing tasks increased to values such that the workload was no longer tolerable for the task; this was also reflected in the increased DIPES rating. An increase in wind speed from 15kts to 25kts for

landings to spot 6 also corresponds with an increase in torque and collective input activity shown in Fig. 18. The pilot commented that at 25kts, on crossing the deck, the aircraft suddenly descended and that on correction with a collective input the pilot reached the torque limit; Fig. 18 shows this incursion over the limit.

Figure 12 shows the highest workload rating was given in a Green 45° WOD during touchdown at spot 6 in a 25kts WOD, which corresponds with a large deviation from the desired longitudinal and lateral position during the descent to touchdown. The range of DIPES suffixes were given as seen in the 15kts wind with the addition of Torque/Engine control (Q). It can also be seen that the final touchdown MTE took longer to execute in the higher wind speed, showing the additional time required by the pilot to complete the task. There was also increased pedal activity as seen in Fig. 21 (b) which shows the 10% control margin was exceeded during the lateral translation and hover, with one occurrence hitting the pedal limit for over 5 seconds to overcome the side-wind component during translation across the deck to spot 6. For spot 6 there was a corresponding increase in workload during hover from 5 to 7 as the wind speed increased from 15kts to 25kts; these higher workload ratings are again consistent with the increased cyclic activity for spot 6 seen in Fig. 27 (b).

C. Green 90°

Referring to the CFD image in Fig. 4 (c) it can be seen that in the 90° wind there is a significant level of turbulence in the horizontal plane above the deck. During the lateral translation, and over spot 5, turbulence is in the region of 20-30%, with significant velocity gradients caused by the flow separating from the starboard deck-edge. Landing to spot 5 in a 15kts Green 90° WOD showed a reduction in overall workload compared with the 15kts Green 45° WOD. No DIPES suffixes were given, reflecting the low workload at this condition.

At 25kts Green 90° WOD there was an increase in workload ratings across all MTEs when landing to spot 5. The pilot commented that sharp gusts, turbulence and erratic disturbances were experienced, leading to acceptance by the pilot of greater deck landing scatter. Significantly, the pilot also found it difficult to maintain heading in the crosswind and exceeded the pedal control limits on a number of occasions shown in Fig. 22 (a), hence the higher DIPES rating in Fig. 13. Causes of the DIPES ratings were ascribed to Yaw control, Turbulence, Forward/Aft positioning and Lateral positioning and, as the pedal limit was reached, a DIPES of 4 was awarded for the overall landing. The difficulty in maintaining heading in the gusting side wind is consistent with the aerodynamic performance envelope of the aircraft which states that the sideward/rearward flight limit is 35kts [49]. The pilot's cyclic activity was consistent with the

Bedford workload ratings in Fig. 13 with an increase from 3 at 15kts to 4 at 25kts for spot 5. The reduced deviation of aircraft position during hover and touchdown at 15 and 25kts compared with the Green 45° case is consistent with the cyclic and pedal activity for this wind direction and shows that the pilot was able to hold position, while at the same time concentrating on heading control due to the lack of pedal authority in the resulting crosswind.

Over spot 6 the turbulence level at hover height is less than 5% but increases towards the deck due the shear layer formed in the air flow separating from the deck edge. There was little change in workload ratings given on landing to spot 6 in a 15kts Green 90° WOD compared with those given at spot 5 for the same conditions. A difference was only seen in the DIPES suffixes given by the pilot which included Yaw control and Forward/aft positioning. The pilot commented that heading accuracy was reduced with a difficult aircraft roll to account for; a large lateral pedal input was also required to maintain heading.

With an increase of WOD speed from 15kts to 25kts on landing to spot 6 an increase in workload was seen, with the highest Bedford workload rating awarded during landing (MTE 3). During this landing task the pilot was unable to maintain heading and the pedal limits were exceeded for 10 seconds during the lateral translation to spot 6 in the 25kts wind as shown in Fig. 22 (b). The pilot also commented that as the spot was behind the ship's aft island it was difficult to judge the deck motion due to a lack of horizon references. The pilot also commented that no lateral eddies were felt over the spot during the hover. The control activity data and aircraft position are consistent with the DIPES ratings awarded in Fig. 13, where in the 25kts wind the pilot awarded a DIPES of 4 because the 10% control margin limits were exceeded and heading accuracy could not be maintained. The causes of the DIPES rating were attributed to Yaw control, Turbulence, Forward/aft positioning, Lateral positioning and Pitch control. Comparing the pilot ratings in the 25kts Green 45° and 90° winds, conducting the landing task required less workload in the 90° wind, due to lower turbulence, but was awarded a higher DIPES due to the erosion of yaw pedal margin which, again, is consistent with the aircraft's aerodynamic performance referred to above.

On landing to spot 6 in a 35kts Green 90° WOD the workload and DIPES ratings show an excessive and intolerable workload for a fleet pilot. Sharp gusts were experienced, causing significant loss of positional accuracy, and were compensated for by the pilot adopting a higher hover altitude. Additional causes of the DIPES in comparison to the 25kts wind included Attitude control and Visual cues. For much of the landing manoeuvre the pedal was against the limit and is the reason why the pilot had to abandon the requirement to maintain a forward-facing heading and instead adopt a 40° heading into wind (again consistent with the aircraft's aerodynamic envelope). Figure 29 shows the

helicopter's heading throughout the entire landing manoeuvre. The time histories are split by vertical dashed lines showing the three MTE's: lateral translation, hover and touchdown. During the lateral translational phase in the 35kts wind the pilot was required to point 40° into the wind to execute the MTE. While heading was recovered somewhat during the hover and landing MTEs, it can be seen that the aircraft still experienced a yaw of up to 10° during the landing MTE.

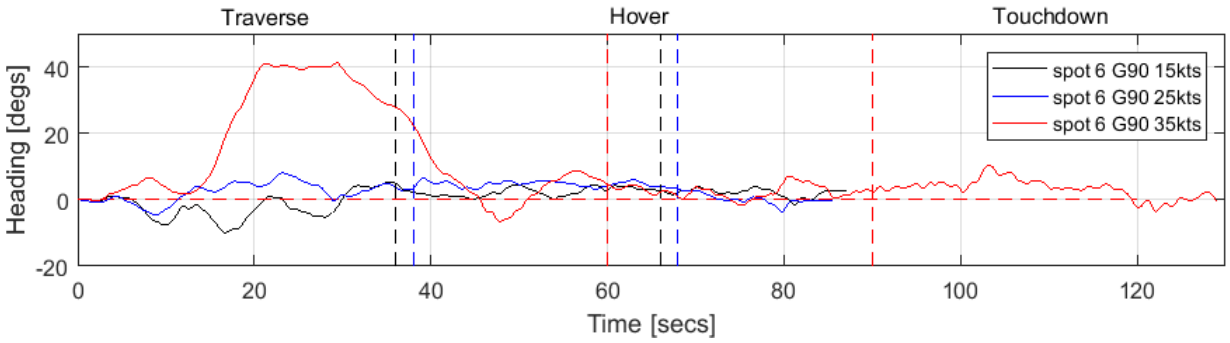

Fig. 29 Helicopter heading in a Green 90° wind at spot 6.

Although the landing was completed and a DIPES 5 awarded, as the pilot was unable to maintain heading the landing should have, in reality, been aborted. Figure 19 shows that the pilot's control activity in collective and torque during the landing task in the Green 90° winds were lower than those seen in the Green 45° winds, consistent with the data shown above for the helicopter position during the landing task. However, as shown in Fig. 29, the pilot was only able to hold position by pointing into the wind and ran out of pedal authority, hence the high DIPES rating in Fig. 13.

V. Closing Remarks and Conclusions

There have been several studies into the application of modelling and simulation to shipboard helicopter operations, e.g. [24, 32, 45]. One fruitful area of research has been the application of piloted simulation in a six degree-of-freedom motion flight simulator, as described in this paper, while another has been the use of software tools that employ pilot models to represent the human pilot, e.g. [50]. These developments, along with studies towards improving the fidelity of the components within the simulation process, such as motion tuning, pilot modelling, coupled rotor/airwake aerodynamics, have focused on meeting the requirements so that simulation can be used to support FOCFTs and SHOL trials. A milestone in this effort was the clearance of the F-35B to HMS Queen Elizabeth, briefly reported in [3]. As discussed earlier in this paper, the clearance process is expensive and the required weather conditions are unpredictable. There is, therefore, a strong case for simulated helicopter deck landings to be adopted to

support at-sea trials by enabling test pilots to explore the limiting envelope before going to sea, not specifically to establish those limits, but to establish where they are likely to be so the time at sea can be used efficiently. Furthermore, if the simulated limits are shown to correspond with those found during the sea trials, then they could provide evidence on how to fill the gaps in the SHOL envelope where wind conditions were not encountered during the period of testing.

A barrier to achieving the benefits described above is that there has so far been no reported systematic comparison, in the public domain, of operational limits and helicopter flight data obtained from deck landings conducted at sea and through simulation. There is, therefore, a pressing need to identify and implement a method to obtain such data so that the techniques such as those described in this paper, and by others, can be beneficially deployed.

Conclusions

This paper has described a series of simulated flight trials where a test pilot has conducted deck landings to the Queen Elizabeth class aircraft carrier in a six degree-of-freedom motion flight simulator configured to represent a Sikorsky SH-60B Seahawk helicopter. This analysis was conducted at the University of Liverpool as part of a larger study into modelling and simulation of the ship-helicopter dynamic interface and did not contribute directly to the helicopter/QEC FOCFTs. The deck landings were conducted in winds from Ahead, and in the challenging winds from Green 45° and Green 90°. The tasks were assessed using pilot workload ratings and control activity, and helicopter trajectory. The main conclusions are as follows:

1. Winds up to 45kts from Ahead presented little difficulty to the pilot when landing to the spots towards the stern of the ship that have been designated for rotorcraft operations. There was a greater level of turbulence observed in the CFD results for spot 6, which is in the lee of the aft island, but even so the workload was not reported as high by the pilot. The level of control activity in cyclic, pedal and collective, and the ability of the pilot to hold a hover position over the spot was consistent with this observation. It can, therefore, be concluded that the designated spots are appropriate for helicopter launch and recovery in a headwind for a wide range of conditions.
2. Conducting a forward-facing landing to spots 5 and 6 in Green 45° winds caused the pilot considerable workload. The pilot deemed that landing to spot 6 was not tolerable for a WOD of 25kts because of a combination of high workload due to turbulence and an inability to maintain heading due to insufficient yaw

control authority. The control activity and positional accuracy was consistent with this observation and showed pedal margins had been exceeded on occasions

3. In a Green 90° beam wind the aircraft again experienced turbulence and insufficient yaw control to maintain heading. However, the pilot was able to conduct the landing task with lower workload than in Green 45° for the same wind speed, but at the expense of heading control, therefore while workload was lower, the DIPES rating was higher.
4. In Green 45° and 90°, the limiting wind speed for the simulated landing was 25kts.
5. The overall synthetic environment, including the integration of CFD airwakes into a real-time piloted simulation, was considered by the pilot to be a realistic representation of the at-sea flying experience. There is a need for flight trials data to compare with simulation to quantify how well simulated deck landings reflect the real-world so the potential benefits of the technology can be realised; this may include important implications for future pilot training.

Acknowledgments

The Authors acknowledge the financial support from the Engineering and Physical Sciences Research Council through an Industrial CASE Award jointly funded with BAE Systems, Ref:1794920, and the ongoing support of ANSYS UK Ltd. The authors would like to thank Dr Steven Hodge for his insight and valuable contribution to the research. The authors would like to thank the pilot, former Empire Test Pilot School Tutor, Andy Berryman, for his professionalism, skill and input during the trials. They would also like to thank Wajih Memon from the Flight Science and Technology research group at the University of Liverpool for his guidance and expertise in the conduct of the simulated trials.

References

[1] Bevilaqua, P. M., "Inventing the F-35 Joint Strike Fighter," *47th AIAA Aerospace Sciences Meeting Including the New Horizons Forum and Aerospace Exposition*, Orlando, Florida, 5-8 January 2009. https://doi.org/10.2514/6.2009-1650

[2] Fry, A., Cook, R., and Revill, N., "CVF ski-jump ramp profile optimisation for F-35B," *The Aeronautical Journal*, 113(1140), 2009 pp. 79-85.

https://doi.org/10.1017/S0001924000002803

[3] Kelly, M. F., Watson, N. A., Hodge, S. J., White, M. D., and Owen, I. "The Role of Modelling and Simulation in the Preparations for Flight Trials Aboard the Queen Elizabeth Class Aircraft Carriers," *14th International Naval Engineering Conference*, Glasgow, 2018.
https://doi.org/10.24868/issn.2515-818X.2018.037

[4] Owen, I., White, M. D., Padfield, G. D., and Hodge S. J., "A virtual engineering approach to the ship-helicopter dynamic interface – a decade of modelling and simulation research at the University of Liverpool," *The Aeronautical Journal*, Vol. 121, Issue 1246, December 2017, pp. 1833-1857.
https://doi.org/10.1017/aer.2017.102

[5] Lumsden, B., and Padfield, G. D., "Challenges at the helicopter-ship dynamic interface," *24th European Rotorcraft Forum*, Marseilles, France, September 1998.

[6] Healey, J. V., "The aerodynamics of ship superstructures," *Proceedings of AGARD Conference D Aircraft Ship Operations*, AGARD-CP-509, France, 1991. pp. 4.1-4.14.

[7] Shukla, S., Sinha, S. S., and Singh, S. N., "Ship-helo coupled airwake aerodynamics: A comprehensive review," *Progress in Aerospace Sciences*, Vol. 106, April 2019, pp. 71-107.
https://doi.org/10.1016/j.paerosci.2019.02.002

[8] Tai, T. C., and Carico, D., "Simulation of DD-963 ship airwake by Navier-Stokes method," *Journal of Aircraft*, Vol. 32, Issue 6, May 2012, pp. 1399-1401.
https://doi.org/10.2514/3.46892

[9] Syms, G. F., "Numerical Simulation of Frigate Airwakes," *International Journal of Computational Fluid Dynamics*, Vol. 18, Issue 2, 2004, pp. 199-207.
https://doi.org/10.1080/10618560310001634159

[10] Reddy, K., Toffoletto, R., and Jones, K. R., "Numerical simulation of ship airwake," *Computers & Fluids*, Vol. 29, Issue 4, May 2000, pp. 451–465.
https://doi.org/10.1016/S0045-7930(99)00033-X

[11] Landsberg, A. M., Boris, J. P., Sandberg, W., and Young, T. R., Jr., "Analysis of the nonlinear coupling effects of a helicopter downwash with an unsteady ship airwake," *33rd Aerospace Sciences Meeting and Exhibit*, Reno, Nevada, 9-12 January 1995.
https://doi.org/10.2514/6.1995-47

[12] Forrest, J. S., and Owen, I. "An investigation of ship airwakes using Detached-Eddy Simulation," *Computers & Fluids*, Vol. 39, Issue 4, April 2010, pp. 656-673.

https://doi.org/10.1016/j.compfluid.2009.11.002

[13] Shipman, J., Arunajatesan, S., Menchini, C., and Sinha, N., "Ship Airwake Sensitivities To Modeling Parameters," *43rd AIAA Aerospace Sciences Meeting and Exhibit*, Reno, Nevada, 10-13 January 2005.
https://doi.org/10.2514/6.2005-1105

[14] Polsky, S., and Bruner, C., "Time-accurate computational simulations of an LHA ship airwake," *18th Applied Aerodynamics Conference*, Denver, Colorado, August 2000.
https://doi.org/10.2514/6.2000-4126

[15] Bardera-Mora, R., García-Magariño, A., Rodríguez-Sevillano, A., and Barcala-Montejano, M. A., "Aerodynamic Flow Effects on Aircraft Carrier Takeoff Performance," *Journal of Aircraft*, Vol. 56, Issue 3, May 2019, pp. 1005-1013.
https://doi.org/10.2514/1.C035188

[16] Watson, N. A., Owen, I., and White, M. D., "Modelling the Effect of Unsteady Turbulent Wakes on a Short Take-off and Vertical Landing (STOVL) Aircraft," *AIAA Aviation 2019 Forum*, Dallas, 17-21 June 2019.
https://doi.org/10.2514/6.2019-3244

[17] Wadcock, A. J., Yamauchi, G. K., Heineck, J. T., Silva, M. J., and Long, K. R., "PIV Measurements of the Wake of a Tandem-Rotor Helicopter in Proximity to a Ship," *AHS 4th Decennial Specialist's Conference on Aeromechanics*, San Francisco, California, January 21-23 2004.

[18] Bardera, R., Rodríguez-Sevillano, A., León-Calero, M., and Nova-Trigueros, J., "Three-dimensional characterization of passive flow control devices over an aircraft carrier ski-jump ramp," *Proceedings of the Institution of Mechanical Engineers, Part G: Journal of Aerospace Engineering*, Vol. 232, Issue 15, 2018, pp. 2737-2744.
https://doi.org/10.1177/0954410017716195

[19] Bogstad, M. C., Habashi, W. G., Akel, I., Ait-Ali-Yahia, D., Giannias, N., and Longo, V., "Computational-Fluid-Dynamics Based Advanced Ship-Airwake Database for Helicopter Flight Simulators," *Journal of Aircraft*, Vol. 39, Issue 5, September 2002, pp. 830-838.
https://doi.org/10.2514/2.3003

[20] Zan, S., "Technical Comment on "Computational-Fluid-Dynamics Based Advanced Ship-Airwake Database for Helicopter Flight Simulation"," *Journal of Aircraft*, Volume 40, Issue 5, September 2003, pp. 1007.
https://doi.org/10.2514/2.6890

[21] Polsky, S., and Naylor, S., "CVN Airwake Modeling and Integration: Initial Steps in the Creation and Implementation of a Virtual Burble for F-18 Carrier Landing Simulations," *AIAA Modeling and Simulation Technologies Conference and Exhibit*, San Francisco, California, 15-18 August 2005.
https://doi.org/10.2514/6.2005-6298

[22] Forrest, J. S., Hodge, S. J., Owen, I., and Padfield, G. D., "Towards fully simulated ship-helicopter operating limits: The importance of ship airwake fidelity," *Proceedings of the American Helicopter Society 64th Annual Forum*, Montréal, Canada, 29 April – 1 May, 2008.

[23] Roper., D. M., Owen, I., Padfield, G. D., and Hodge, S. J., "Integrating CFD and piloted simulation to quantify ship-helicopter operating limits," *The Aeronautical Journal*, Vol. 110, Issue 1109, July 2006, pp. 419-428. https://doi.org/10.1017/S0001924000001329

[24] Hodge, S. J., Forrest, J. S., Padfield, G. D., and Owen, I., "Simulating the environment at the helicopter-ship dynamic interface: research, development and application," *The Aeronautical Journal*, Vol. 116, Issue 1185, November 2012, pp. 1155-1184. https://doi.org/10.1017/S0001924000007545

[25] Forrest, J. S., Kääriä, C. H., and Owen, I., "Evaluating ship superstructure aerodynamics for maritime helicopter operations through CFD and flight simulation," *The Aeronautical Journal*, Vol. 120, Issue 1232, October 2016, pp. 1578-1603. https://doi.org/10.1017/aer.2016.76

[26] Kääriä, C. H., Forrest, J. S., and Owen, I., "The virtual AirDyn: A simulation technique for evaluating the aerodynamic impact of ship superstructures on helicopter operations," *The Aeronautical Journal*, Vol. 117, Issue 1198, December 2013, pp. 1233-1248. https://doi.org/10.1017/S0001924000008836

[27] White, M. D., Perfect, P., Padfield, G. D., Gubbels, A. W., and Berryman, A. C., "Acceptance testing and commissioning of a flight simulator for rotorcraft simulation fidelity research," *Proceedings of the Institution of Mechanical Engineers, Part G: Journal of Aerospace Engineering*, Vol. 227, Issue 4, April 2013, pp. 663 – 686. https://doi.org/10.1177/0954410012439816

[28] Du Val, R.W., and He, C., "Validation of the FLIGHTLAB virtual engineering toolset," *The Aeronautical Journal*, Vol. 122, Issue 1250, April 2018, pp. 519-555. https://doi.org/10.1017/aer.2018.12

[29] Howlett, J. J., "UH-60A Black Hawk Engineering Simulation Program: Volume I – Mathematical Model," NASA-CR-166309, December 1981.

[30] Carico, G. D., Fang, R., Finch, R. S., Geyer Jr., W. P., Cdr. (Ret.) Krijns, H. W., and Long, K., "Helicopter/Ship Qualification Testing," *RTO AGARDograph 300 Flight Test Techniques Series*, Vol. 22, Research and Technology Organisation, NATO, France, February 2003, pp. 1-126.

[31] Hoencamp, A. “An Overview of SHOL Testing Within The Royal Netherlands Navy,” *35th European Rotorcraft Forum*, Hamburg, Germany, 22-25 September 2009.

[32] Advani, S. K., and Wilkinson, C. H. “Dynamic interface modelling and simulation – a unique challenge,” *Royal Aeronautical Conference on Helicopter Flight Simulation*, London, November 2001.

[33] Memon, W. A., Owen, I., and White, M. D. "Motion Fidelity Requirements for Helicopter-Ship Operations in Maritime Rotorcraft Flight Simulators," *Journal of Aircraft*, August 10, 2019. https://doi.org/10.2514/1.C035521

[34] Watson, N. A., Kelly, M. F., Owen, I., Hodge, S. J., and White, M. D. “Computational and experimental modelling study of the unsteady airflow over the aircraft carrier HMS Queen Elizabeth,” *Ocean Engineering*, Vol. 172, January 2019, pp. 562-574. https://doi.org/10.1016/j.oceaneng.2018.12.024

[35] Watson, N. A., Owen, I., and White, M. D. “Experimental Validation of the Unsteady CFD-generated Airwake of the HMS Queen Elizabeth Aircraft Carrier,” *AIAA Aviation 2019 Forum*, Dallas, 17-21 June 2019. https://doi.org/10.2514/6.2019-3029

[36] Spalart, P. R., Deck, S., Shur, M. L., Squires, K. D., Strelets, M. Kh., and Travin, A. “A New Version of Detached-Eddy Simulation, Resistant to Ambiguous Grid Densities,” *Theoretical and Computational Fluid Dynamics*, Vol. 20, Issue 3, May 2006, pp. 181-195. https://doi.org/10.1007/s00162-006-0015-0

[37] Spalart, P. R., Jou., W. H., Strelets, M., and Allmaras, S. R., “Comments on the feasibility of LES for wing and on a hybrid RANS/LES approach,” *1st ASOSR Conference on DNS/LES*. Arlington, TX, 4-8 August 1997

[38] Garratt, R., *The Atmospheric Boundary Layer*, Cambridge Atmospheric and Space Science Series, Cambridge University Press, 1992.

[39] Polsky, S., “CFD Prediction of Airwake Flowfields for Ships Experiencing Beam Winds,” *21st AIAA Applied Aerodynamics Conference*, Orlando, Florida, 23-26 June 2003. https://doi.org/10.2514/6.2003-3657

[40] Denham, J. W., Krumenacker, J. L., D’Mello G. W., and Lewis, M., “Taking advanced STOVL flight control to sea: The VAAC follow-on research programme,” *American Helicopter Society Aerodynamics, Acoustics, and Test and Evaluation Technical Specialists Meeting*, San Francisco, California, 23-25 January, 2002.

[41] Bardera-Mora, R., Calero, M. L., and García-Magariño, “Aerodynamic effect of the aircraft carrier island on flight deck flow with cross wind,” *Proceedings of the Institution of Mechanical Engineers, Part M: Journal of Engineering for the Maritime Environment*, Vol. 232, Issue 2, January 2017, pp. 145-154.

https://doi.org/10.1177/1475090216689172

[42] Watson, N. A., Kelly, M. F., Owen, I., and White, M. D., "The Aerodynamic Effect Of An Oblique Wind On Helicopter Recovery To The Queen Elizabeth Class Aircraft Carrier," *Vertical Flight Society's 75th Annual Forum & Technology Display*, Philadelphia, Pennsylvania, 13 – 16 May, 2019.

[43] Scott, P., White, M. D., and Owen, I. "The Effect of Ship Size on Airwake Aerodynamics and Maritime Helicopter Operations," *41st European Rotorcraft Forum*, Munich, 1-4 September 2014.

[44] Crozon, C., Steijl, R., and Barakos, G. N., "Numerical Study of Helicopter Rotors in a Ship Airwake," *Journal of Aircraft*, Vol. 51, Issue 6, December 2014, pp. 1813-1832.
https://doi.org/10.2514/1.C032535

[45] Oruc, I., Horn, J. F., Shipman, J., and Polsky, S., "Towards real-time pilot-in-the-loop CFD simulations of helicopter/ship dynamic interface," *International Journal of Modeling, Simulation, and Scientific Computing*, Vol. 8, Issue 4, 2017.
https://doi.org/10.1142/S179396231743005X

[46] McTaggart, K., "Validation of ShipMo3D Version 1.0 User Applications for Simulation of Ship Motion," Technical Memorandum, DRDC Atlantic TM 2007-173, August 2007.

[47] Roscoe, A., and Ellis, G. "A Subjective Rating Scale for Assessing Pilot Workload in Flight: A decade of Practical Use," RAE report TR90019, Royal Aircraft Establishment, Farnborough, UK, March 1990.

[48] Ministry of Defence, "Defence Standard 00-133 Part 3 Issue 2 Aviation Arrangements in Surface Ships: Design, Construction and Provision (Flight Deck)," UK Ministry of Defence, 21 August 2015.

[49] NATOPS Flight Manual Navy Model SH-60B Helicopter, A1-H60BB-NFM-000, April 2008.

[50] Polsky, S. A., Wilkinson, C., Nichols, J., Ayers, D., Mercado-Perez, J., and Davis, T. S., "Development and Application of the SAFEDI Tool for Virtual Dynamic Interface Ship Airwake Analysis," *54th AIAA Aerospace Sciences Meeting*, San Diego, California, 4-8 January, 2016.
https://doi.org/10.2514/6.2016-1771